Low Voltage Ride-Through for Indirect Matrix Converter Based Open-End Winding Drives

A DISSERTATION
SUBMITTED TO THE FACULTY OF
UNIVERSITY OF MINNESOTA
BY

Santhosh Krishnamoorthi

IN PARTIAL FULFILLMENT OF THE REQUIREMENTS
FOR THE DEGREE OF
DOCTOR OF PHILOSOPHY

ADVISER: Prof. Ned Mohan

August 2017

Acknowledgements

I would like to express my earnest gratitude to my adviser Prof. Mohan for giving me an opportunity to be a part of his research group and learn a great deal over six years. I am thankful for his ideas and support without which this journey would have been impossible. Thank you!

I would also like to thank Prof. Robbins, Prof. Wollenberg, Prof. Dhople and Prof. Rajamani for being a part of my committees and for giving me valuable feedback about my work.

I gratefully acknowledge the funding agencies, Office of Naval Research (ONR) and University of Minnesota Center for Electric Energy (UMCEE) for supporting me through the years.

For being always there, for being a sounding board and helping me with work and beyond, I thank my dear friend, Siddharth who has constantly pushed me to achieve this. I would also like to thank Saurabh for guiding me with all my work and for being a good friend through this journey. My heartfelt thanks to Srikant, Ashish, Rohit, Eric and David who have been the best lab mates and friends and made this a great experience and thanks to Shankernarayan who helped me through the initial stages. A special thanks to Ruben and Kartik for making it a delightful one.

Finally, thanks to my sister who has been supportive throughout my life and am eternally grateful to my parents for everything.

Dedication

To all the teachers who taught me valuable lessons

Abstract

Adjustable speed drives (ASD) are one of the major load components in power systems and with the advent of wide band gap devices, which provide efficiencies greater than 95%, variable frequency drives will continue to grow and integrate into the systems. ASDs serve a varied set of processes including HVACs, oilrigs and recently many electric vehicles (EV). The most commonly employed types are the DC-to-AC or AC-to-AC drives with DC/AC drives being more popular in storage and EV applications. AC/AC drives have been dominated by converters using large capacitors with DC bus viz. back-to-back converters. These converters are becoming more reliable and have been tested with new advancements in the industry. In addition, the DC bus capacitor provides an inbuilt energy storage mechanism, which could be used for ride-through operations during fault conditions. In some applications like wind turbines, the presence of large capacitive and reactive components in the drive could be a drawback due to lesser reliability and increased weight. Hence, converters that eliminate the need for large capacitors (viz. cycloconverters and matrix converters) are advantageous in such applications. Matrix converters (MC) have been in research and development for almost three decades, and several topologies and new modulation techniques have been proposed. In addition to elimination of the bulky DC bus capacitor, MCs provide sinusoidal input and output waveforms with lesser harmonics, and have inherent bi-directional power flow capability while offering full input power factor control. In industry, MCs are produced by few manufacturers and is still a niche product.

High frequency common mode voltage (CMV) switching is a by-product of the ASDs operating at medium to high frequencies and cause bearing currents to flow, which damage the machine and reduce their lifetime. Elimination or reduction of common mode voltage is a well-researched topic and it has been addressed with plenty of solutions for different kind of drives. One of the recently developed solution is the usage of open-end winding drive modulated using rotating space vectors. Open-end winding machine is constructed by opening the shorted side of an induction machine, which is supplied by another similar converter. Different types of converters including MCs have been used to construct this drive. Matrix converter based open-end winding drive have two types

including direct and indirect matrix converter based drives and, this dissertation concentrates on the usage of a three-level indirect matrix converter based open-end winding.

It is important that the ASDs are reliable and dependable during fault conditions in the power system. They should be able to ride-through the fault, supply the losses, and maintain the flux in the motor since re-building it could affect the operations. System faults could create over-voltages or voltage sags (sags are more frequent than over-voltages) and many commercial drives address the voltage sag problem with a ride-through solution for up to 30 cycles of interruption. Ride-through solutions include usage of storage devices, modification of the drive or use of inherent kinetic energy.

Matrix converters lack an inbuilt storage device and modification of the drive could be expensive. This dissertation proposes a low voltage ride-through method for a three-level indirect matrix converter based open-end winding drive using the input filter capacitor. The three-level indirect MC drive has an advantage over other matrix converter based drives, that it can provide a ride-through solution without the need for modifications or addition of storage devices. The input filter capacitor on the three-level bus between the front-end converter and the two three level inverters is used as the voltage source during the fault while its voltage is maintained by using the kinetic energy from the motor. This is achieved by modification of control loops in a traditional vector control configuration to control the capacitor voltage by drawing power from the motor.

In summary, this dissertation describes a three-level indirect matrix converter for an open-end winding drive to eliminate the high frequency common-mode voltage, and proposes a low voltage ride-through method for the operation of the drive during fault conditions using the input filter capacitors as an energy transfer device. The method has been presented with detailed derivations and analyses and been verified using simulations and experimental results using a two-level inverter drive.

Contents

List of Tables

List of Figures

Chapter 1

Introduction

Adjustable Speed Drives are one of the most important applications of power electronics. With different types of adjustable speed drives in existence, they many industries including oil and gas, HVAC, pumps etc. With the prevalence of the drives, its protection and operation under abnormal conditions are also important. The work presented in this dissertation addresses the issue for a three-level indirect matrix converter based open-end winding drive. A low voltage ride-through solution using the input filter capacitor for the above-mentioned drive is proposed and demonstrated in this work.

This chapter discusses different types of adjustable speed drives and focusses on matrix converter drives in detail with emphasis on open-end winding drives. Further, different types of ride-through existing methods are discussed briefly followed by a short description of the proposed method and its advantages over the other methods. Finally, the contributions and the organization of the dissertation is presented.

1.1 Adjustable speed drives

The use of adjustable speed drives (ASD) in modern day industrial applications has been very widespread and is increasing with the integration of renewable energy sources into the grid and other applications like electric vehicles. ASDs could employ different kinds of converters depending on the type of the input source and the type of the load. For example, in electric vehicles, with the use of large batteries, inverters (DC to AC) are used to drive the induction or permanent magnet AC machines. In applications where the source is also AC, back-to-back converters, cycloconverters or matrix converters are utilized. This section will discuss about the different types of AC-to-AC converters viz., back-to-back converters, matrix converters and matrix converters for open-end winding drive.

1.1.1 Back-to-Back converter drives

Back-to-back converters comprises of two components: a rectifier, which can be diode-based or active (using IGBTs) depending on the application. An active rectifier front-end allows bi-directional power flow operations [1]. The rectifier connects the input to a DC bus with a very large capacitor, which filters out the current/torque ripples. The DC bus supplies an inverter that drives the machine. A typical back-to-back converter is shown in Fig 1.1. These are commonly employed type of converters in the industrial applications given its flexible configuration, simple feedback control of input currents etc. The presence of the large DC bus capacitor enables inherent energy storage, which can be used during extended low voltage ride-through operations [2].

One of main drawbacks of this type of converter is its bulkiness [4] and long-term reliability [3] due to the presence of the large DC bus capacitor. In some applications like, wind turbines, this converter could increase the weight. Cycloconverters provide a solution for the bulkiness of the back-to-back converters through the elimination of the DC bus capacitor. Matrix converter is a special type of cycloconverter, which directly connects the input to the output. These types of converters are described in the next subsection.

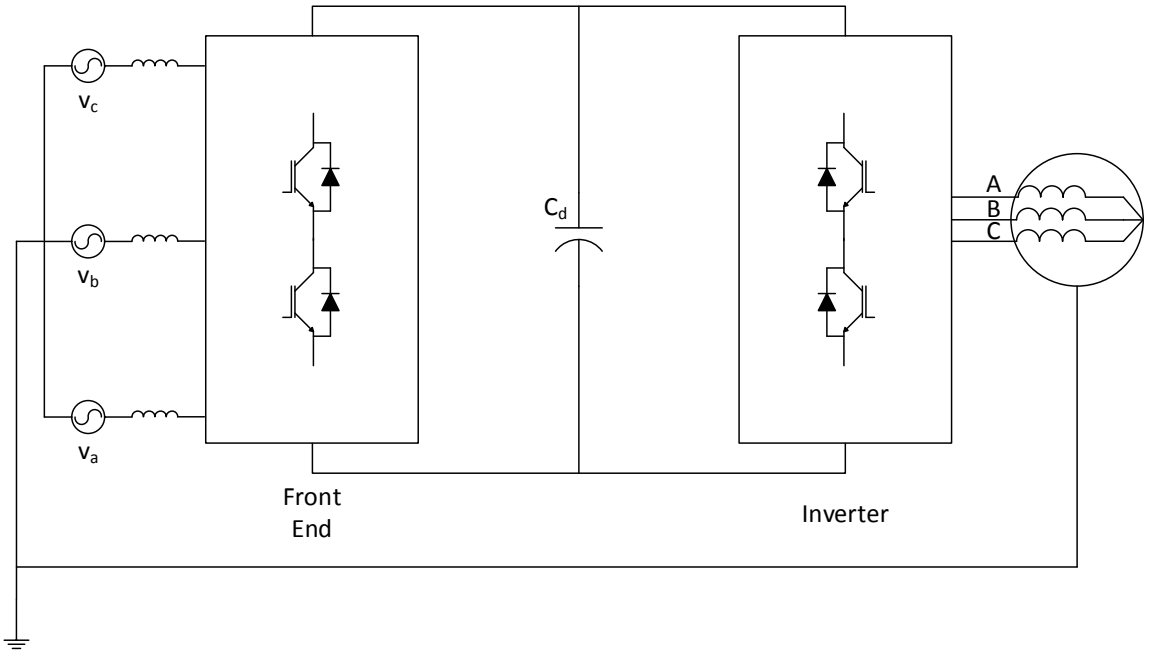

Fig 1.1 Back to back converter based ASD

1.1.2 Matrix converter drives

Matrix converters (MC) were first introduced by Venturini [5] in 1980 with the need to reduce the use of reactive elements. Since then many derived topologies and different modulation strategies have been proposed and implemented for matrix converters [6]–[12]. In addition to reduction in size, MCs have reduced total harmonic distortion (THD) and draw sinusoidal input currents from the grid. In general, matrix converters are classified into two types as direct matrix converters and indirect matrix converters.

Direct matrix converters connect the three input phases to the output directly through a set of semiconductor bi-directional switches. A conventional direct matrix converter drive is shown in Fig 1.2. Since its introduction, several developments have been made using the direct matrix converter topology [13]-[16].

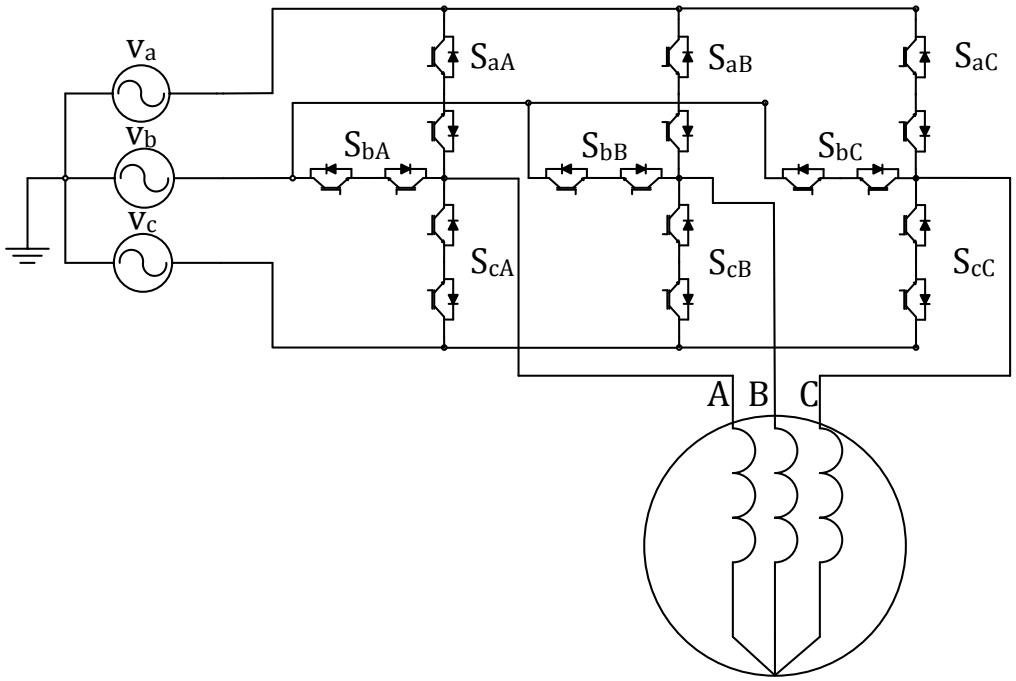

Fig 1.2 Direct Matrix Converter based Single-Ended Drive

Indirect matrix converters have a rectifier stage and an inverter stage with a virtual DC link connecting the two stages. The advantage of this topology is that it can be realized using six bi-directional switch modules and a traditional inverter module unlike the direct matrix converter, which needs nine bi-directional switch modules. Another common way to operate the matrix converter is by using indirect modulation strategy. Two transformations viz. rectifier and inverter transformations are calculated and combined to produce the desired output [17].

In general, the high frequency operation of ASDs create a high frequency common mode voltage switching in the machine. This is propagated to the machine through the parasitic capacitance between the stator and the ground. The ground is common to the machine and the converter, and the high frequency components produced by the switching of the converter. This creates a high frequency common mode voltage switching across the bearings and produces bearing currents, which over time, damage the bearings in the machine and reduce their lifetime. Many methods for elimination of common mode voltage in ASDs are discussed in the literature including usage of active filters [18] & [19], implementation of alternate topologies [20] & [21] and modified modulation strategies [22]

& [23]. One of the methods to eliminate common mode voltage in a matrix converter based drive is by modifying it using two matrix converters feeding an open-end winding machine and modulating it using rotating space vectors as described briefly in the following section.

1.1.3 Open-end winding drives

Adjustable speed drives for open-end winding have been in development for over a decade and many topologies have been proposed and implemented. The usage of matrix converter in open-end winding drives was first introduced by Mohapatra [24] and further researched in [25] & [26]. Similar to matrix converter drives in 1.1.1, the open-end winding drives are also classified into direct and indirect matrix converter drives.

The direct matrix converter based open-end winding drive uses two direct matrix converters to connect the three-phase input to the two ends of the open-end winding machine. The indirect matrix converter has a front-end that converts the three-phase input to a three-level voltage (max-mid-min) while switching at line frequency. These three-level voltages are the input for the two three-level inverters, which feed the open-end winding machine. The direct and indirect matrix converter based open-end winding drives are shown in Fig. 1.3 and 1.4 respectively.

These drives are modulated using space vectors and only the rotating vectors in the set of 27 available vectors are used. These rotating vectors make sure that every input phase is always connected to an output phase hence there will be no common-mode voltage to the ground since all three voltages produced at the machine add up to zero. This is further explained in chapter 2.

In particular, the research discussed in this dissertation uses the three-level indirect matrix converter topology due to its advantages over the direct matrix converter based drive. Two major advantages are no requirement for clamp circuit and lower losses since the front-end converter is operated at line frequency. In addition, this converter can also be used to disconnect the drive from the grid if a fault occurs and the filter capacitors connected between the three busses are used as voltage source for the two inverters during the ride-through operation. Chapter 3 presents this method in detail.

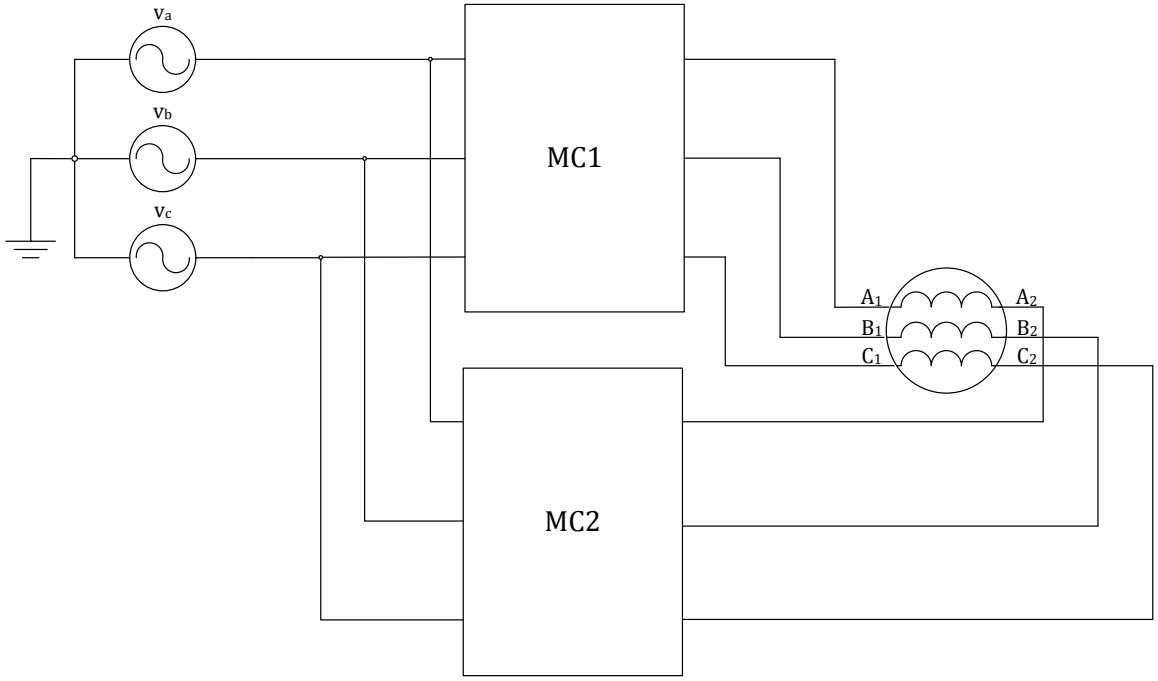

Fig 1.3 Direct Matrix Converter based Open-End Winding Drive

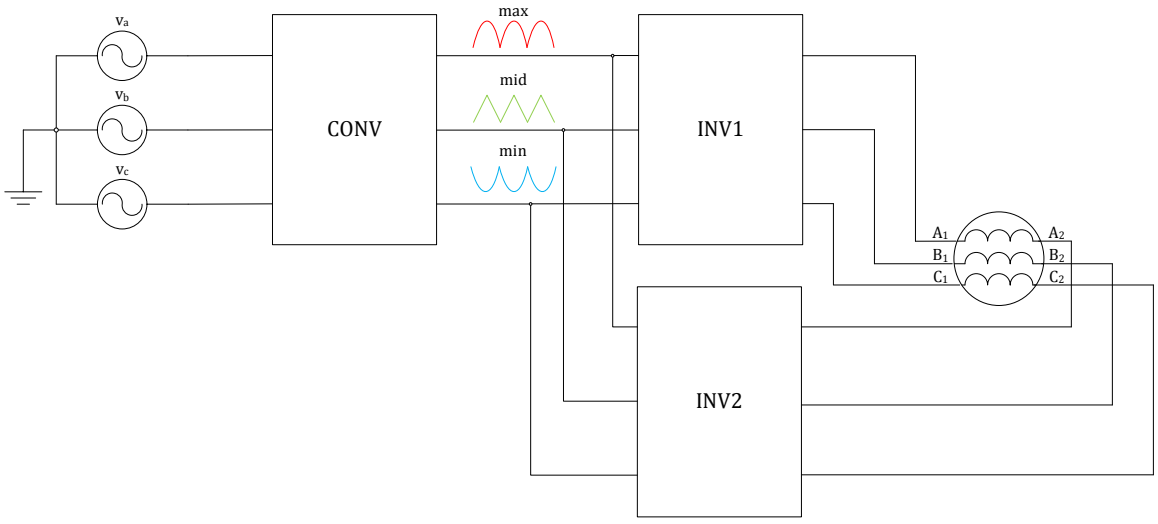

Fig 1.4 Three-Level Indirect Matrix Converter Based Open-End Winding Drive

1.2 Voltage sags in power systems and ride-through for adjustable speed drives

Voltage sags are commonly caused by faults occurring in the power systems in transmission lines, transformers, feeders etc. Sags are defined as reduction in the grid voltage between 0.1 pu to 0.9 pu for 0.5s to 1 min [27]. Single-phase to ground fault, two phase and three phase to ground faults are the common faults with single phase being the very frequently occurring type of fault and has more than 80% of the share of the total faults [28]. There are four types of voltage sags (type A, B, C and D) [29]. Type A and B sags are associated only with the change in the magnitude of the three-phase voltages (type A – all three phases, type B – one of the phases) and type C and D sags are associated with both reduction in magnitude and change in the phase angle. Voltage sags could propagate from one area of the power system to another and the type of fault could change based on the types of transformers the fault is propagated through [30].

Adjustable speed drives are very sensitive to these voltage sags and could trip within a cycle of a fault creating a sag only up to 0.85 pu [31]. Tolerance to faults is one of the most important aspects in a commercial ASD - operation of ASDs under fault conditions is essential to make it dependable in the field and a number of solutions have been proposed in literature [32]-[34]. Without ride-through in ASDs, a grid fault would result in motor flux decay and eventual process interruption. Ride-through operation in ASDs generally use three main approaches [35]. One is through usage of additional storage device *viz*. supercapacitors, flywheels, battery backup systems etc. The second method uses the rotational kinetic energy of the motor-load assembly during the fault to maintain the flux; and the third approach is realized through modification of hardware e.g. replacing the diode rectifier with an active front-end rectifier (in a back-to-back converter) etc.

Implementation of a ride-through method for matrix converter drives is challenging due to the lack of inherent energy-storage unlike traditional back-to-back converters. Various ride-through approaches for matrix converter based drives have been introduced previously. Cha et al. [36] proposed a method using additional switches and storage capacitors to operate it as a conventional PWM-inverter to supply the losses and maintain

the motor flux during the fault. Other techniques include, clamp circuit utilization with zero vectors [37] and a reduced speed reference scheme, proposed by Wiechmann [38].

1.2.1 Ride-through method using filter capacitor

This dissertation presents a low-voltage ride-through technique for the three-level indirect matrix converter drive [39] similar to a method used in [40] for a direct matrix converter drive using additional disconnect switches. In this approach, the rotational kinetic energy in the motor is used to maintain the voltages in the input filter capacitors during the fault condition. The capacitors are used as the new voltages sources for the three-level inverters to sustain the motor flux and losses. The energy transfer between the different components of the drive is depicted in Fig. 1.5. The motor is vector controlled [41] under normal conditions and after the occurrence of a fault; the speed control loop is replaced by a voltage control loop to regulate the filter capacitor voltages. The flux control remains unchanged. The drive is disconnected from the grid by turning off the IGBTs in the front-end converter and when the fault is cleared, the normal operation is resumed using a reconnection strategy that will reduce current transients and reaccelerates the motor seamlessly. The salient advantages of the presented ride-through method are:

- Does not require additional energy storage devices to maintain the motor flux
- No modification of hardware or addition of extra semiconductor switches is required

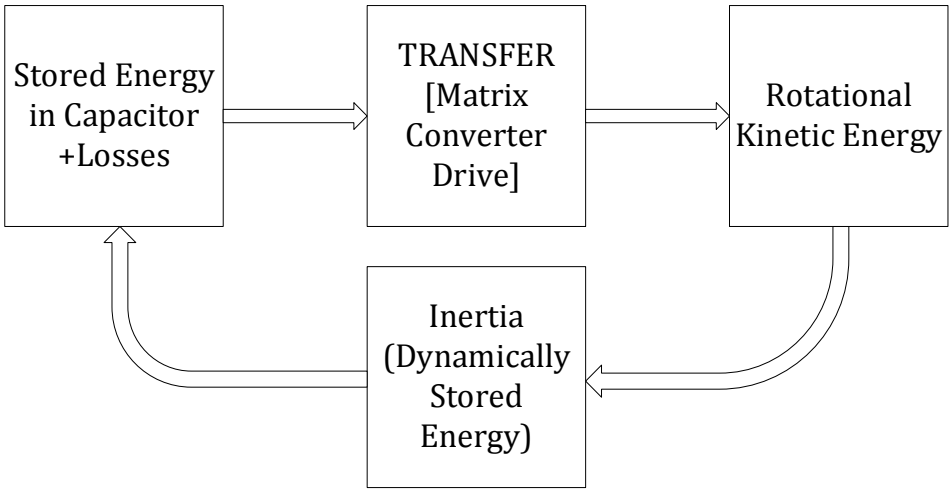

Fig 1.5 Energy Transfer Mechanism for the proposed ride-through method using Filter Capacitors for an Indirect Matrix Converter based Open-End Winding Drive

1.3 Organization of the dissertation

This dissertation is organized into four chapters. The chapter contents are described below:

- Chapter 1 introduces the topic and describes different types of adjustable speed drives used in the industry followed by brief description of the matrix converter based open-end winding drive. Finally, the different types of voltage sags and the available ride-through methods are discussed. The proposed ride-through method is introduced and presented briefly.
- Chapter 2 presents the space vector pulse width modulation method using rotating vectors followed by the detailed descriptions of direct and indirect matrix converter based open-end winding drives. The chapter is concluded with simulation results of operation of the matrix converter based open-end winding drive using the mentioned modulation method.
- Chapter 3 proposes a ride-through strategy for three-level indirect matrix converter based open-end winding drive using filter capacitors followed by a description of the sequence of events for its implementation. Simulation results are presented as a validation for the proposed method. Finally, an experimental setup built using a two-level inverter drive to demonstrate the method is presented with results.
- Chapter 4 presents the conclusions drawn from the work for this dissertation and provides ideas for future research on the topic.

Chapter 2

Rotating Space Vector Modulated Three-Level Indirect Matrix Converter Based Open-End Winding Drive

Space-Vector Pulse Width Modulated direct and indirect matrix converters is a well-researched topic as discussed in Chapter 1. The direct and indirect matrix converter based open-end winding drives have also been widely discussed in literature [42] & [43]. This chapter describes about the topology, strategy and operation of the indirect matrix converter based open-end winding drive. The simulation results of the drive using a mathematical model of an induction motor are also shown.

The conventional matrix converter drives make use of the stationary and zero vectors, which, generates non-zero common mode voltage switching at the motor terminals and induces bearing currents and increases Electromagnetic Interference (EMI). By making use of rotating space vectors for the drive, the common-mode voltage switching is reduced. The generation of voltage using rotating vectors is briefly discussed and a strategy is presented to show how the three-level indirect matrix converter based drive can generate up to 1.5 times the input voltage at the motor terminals and control the power factor within a certain range.

2.1 Matrix Converter based open-end winding drives

Matrix converter topologies for open-end winding drives have been in research for over a decade since its introduction. One of the main advantages of the drive is reduction of common mode voltages. Common mode voltages produce bearing currents, which cause EMI. This is a widely known problem in Adjustable speed drives (ASD) and several methods to reduce or eliminate them have been proposed previously including usage of active filters, alternate distribution of zero vectors in sampling period [12] etc. Common-mode voltages are often caused by usage of stationary and zero vectors due to asymmetrical connection between the input and output phases. Rotating vectors eliminate that problem by ensuring that every input phase is always connected to an output phase. The main drawback of using rotating vectors is lower output gain compared to when the stationary vectors are used. This is overcome by using two matrix converters feeding an open-end winding induction motor. Two types of matrix converter based open-end winding drives have been proposed:

- Direct matrix converter based open-end winding drive: Two direct matrix converters connected to open-end winding machine
- Indirect three-level matrix converter based open-end winding drive: A front-end converter and two three-level converters connected to open-end winding machine

The switching using the rotating vectors and both types of matrix converter drives are discussed below in the following sub-sections.

2.1.1 Direct matrix converter based open-end winding drive

The detailed topology of a direct matrix converter drive with open-end winding machine is shown in Fig. 2.1. The topology is made of two direct matrix converters connecting the three-phase input to the open-end winding machine. The drive is constructed using 18 bi-directional IGBTs. The two matrix converters are switched by employing the space-vector PWM method using only the rotating vectors. The usage of rotating vectors make sure that always all the input phases are connected to an output phase. This eliminates the generation of high frequency common mode voltage as shown in (2.1).

The detailed description and the strategy of switching using rotating vectors in SVPWM is presented in the next section.

$$v_{cm} = \frac{v_A + v_B + v_C}{3} = 0 \tag{2.1}$$

2.1.2 Space vector PWM using rotating vectors for matrix converter based open-end winding drives

Space vector pulse-width modulation (SVPWM) is the most commonly used technique for switching matrix converter drives. The method is implemented using vectors which represent the connection between the input and output phases. Based on the combinations there are 27 vectors. The vectors are divided into two categories as:

- Stationary and zero vectors – These are a set of 21 vectors, which are located along the diagonals and center of a regular hexagon with amplitude varying from $0\ to\ \sqrt{3}V_i$ where V_i is the input voltage amplitude. (3 x $\vec{v}_0$ and $\vec{v}_1$ to $\vec{v}_{18}$)
- Rotating vectors – These are six vectors rotating with a frequency of $\omega_i\ (= 2\pi f_i)$ where f_i is the frequency of the input voltage to the drive. These vectors rotate either in clockwise direction or counter-clockwise direction with an amplitude of $\frac{3}{2}V_i$. (Counter-clockwise rotating (CCW): $\vec{v}_{abc}$, $\vec{v}_{bca}$, $\vec{v}_{cab}$, Clockwise rotating (CW): $\vec{v}_{acb}$, $\vec{v}_{cba}$, $\vec{v}_{bac}$)

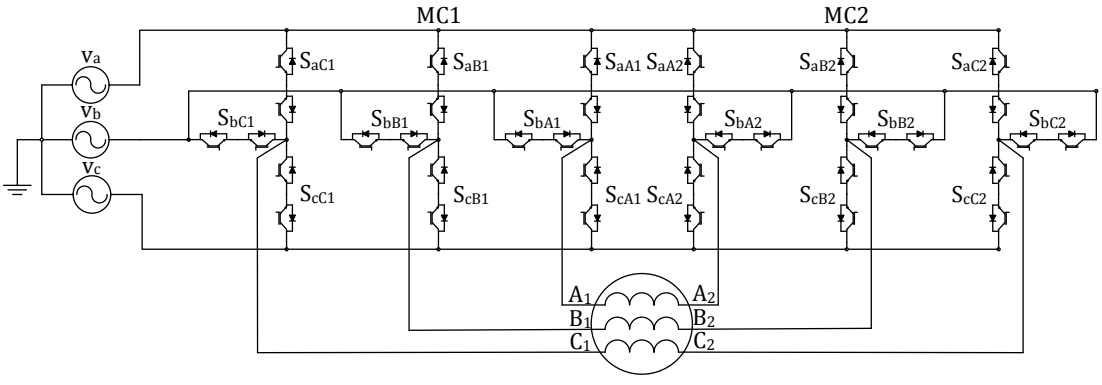

Fig 2.1 Detailed topology of direct matrix converter based open-end winding drive

Conventionally, matrix converter drives are switched only using the stationary and zero vectors in SVPWM method where, the duty ratios for each sector are computed for two stationary vectors and the zero vector. The theoretical maximum limit for the output voltage amplitude using the stationary and zero vectors is $0.866\,V_i$. On the other hand, SVPWM using only rotating vectors has a theoretical limit of only $0.5\,Vi$ for generated output voltage amplitude as shown in Fig. 2.2 (a). This disadvantage is overcome in the open-end winding matrix converter drive by using two matrix converters to generate the output voltage. A gain of up to $1.5V_i$ is achieved by using two matrix converters in the drive. Fig 2.2 (b) shows the generation of output voltage using rotating vectors in a single-end winding drive and an open-end winding drive. The resultant output voltage is given as

$$\vec{v}_{oe}(t) = \vec{v}_{mc_1}(t) - \vec{v}_{mc_2}(t) \tag{2.2}$$

Where, $\vec{v}_{mc_1}(t)$ and $\vec{v}_{mc_2}(t)$ are the individual output voltages generated by the two matrix converters using the rotating vectors. The duty ratios for modulation are generated by using $\vec{v}_{mc_1}(t)$ and $\vec{v}_{mc_2}(t)$ as the reference voltages. With respect to Fig. 2.2 (b) where if only the CCW vectors are used, $\vec{v}_{mc_1}(t)$ and $\vec{v}_{mc_2}(t)$ correspond to $\vec{v}_{ccw_1}$ and $\vec{v}_{ccw_2}$ respectively. At every time step (T_s) of the switching cycle, one matrix converter is switched using a constant level reference voltage and the other matrix converter is modulated using the difference between output voltage and the constant level reference voltage. For instance, at a particular time step of the switching cycle, $\vec{v}_{mc_1}(t)$ will be held at a constant reference, $\vec{v}_{abc}$ and $\vec{v}_{mc_2}(t)$ will be equal to $\vec{v}_{oe} - \vec{v}_{abc}$. The pulses are now generated by using $\vec{v}_{abc}$ as reference for MC1 and $\vec{v}_{oe} - \vec{v}_{abc}$ as reference for MC2. Similarly, depending on the sector, the constant vector is chosen from one of the CCW rotating or CW rotating vectors. In addition, the constant voltage reference vector selection is alternated between MC1 and MC2 in every consecutive sector.

The sector is determined by using both the angles of the input voltage phasor and the output voltage phasor. For CCW rotating vectors, the sector is determined by using $\angle v_o - \angle v_i$ and for CW rotating vectors, the sector is determined using $\angle v_o + \angle v_i$. The duty ratio calculations are shown in equations (2.3) and (2.4)

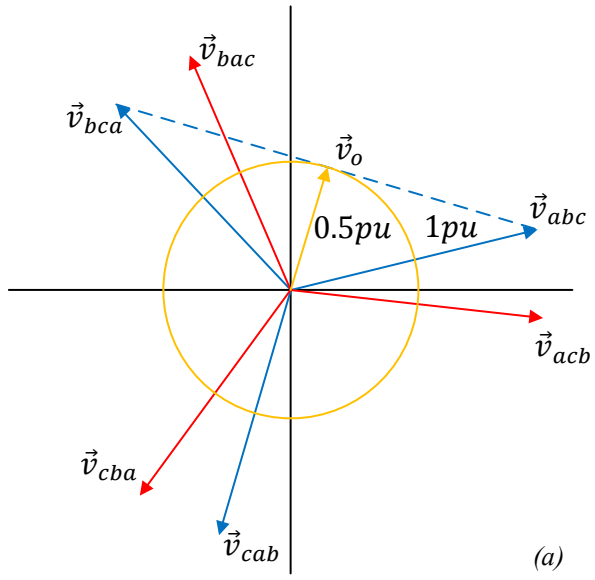

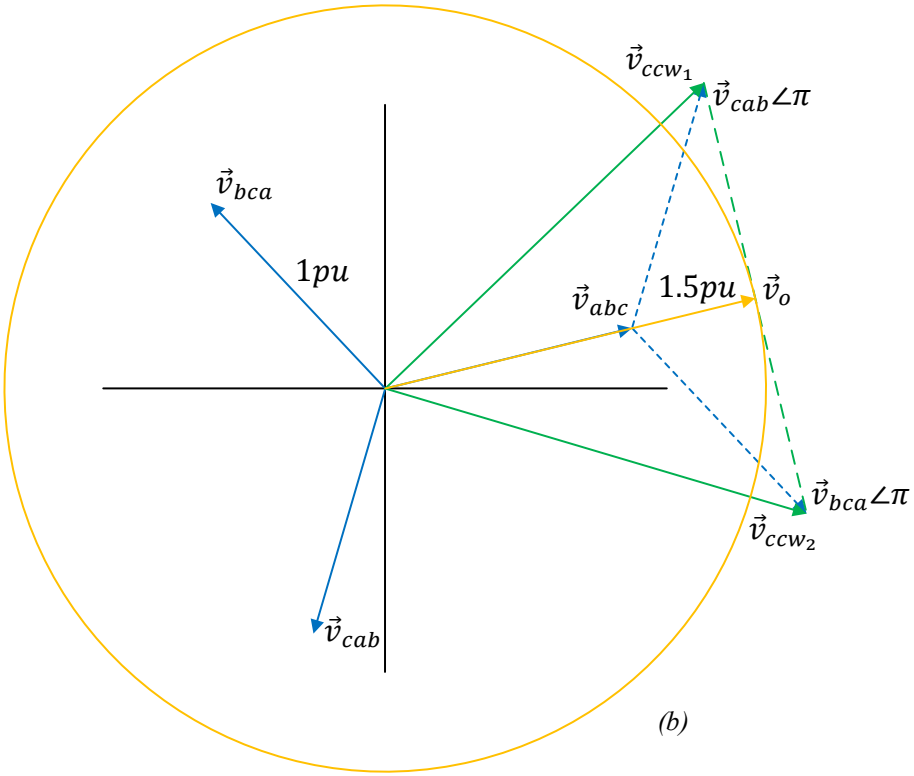

Fig 2.2 Generation of output voltage using rotating vectors in (a)Single-end winding machine and (b)Open-end winding machine

$$\frac{3}{2}\hat{v}_o e^{j\omega_o t} = \frac{3}{2}\hat{v}_i(\lambda_1 e^{\pm j\omega_i t} + \lambda_2 e^{\pm j(\omega_i t - 2\pi/3)} + \lambda_3 e^{\pm j(\omega_i t + 2\pi/3)}) \quad (2.3)$$

$$\begin{bmatrix} m\cos\omega_o t \\ m\sin\omega_o t \\ 1 \end{bmatrix} = \begin{bmatrix} \cos\omega_i t & \cos\left(\omega_i t - \frac{2\pi}{3}\right) & \cos\left(\omega_i t + \frac{2\pi}{3}\right) \\ \pm\sin\omega_i t & \pm\sin\left(\omega_i t - \frac{2\pi}{3}\right) & \pm\sin\left(\omega_i t + \frac{2\pi}{3}\right) \\ 1 & 1 & 1 \end{bmatrix} \begin{bmatrix} \lambda_1 \\ \lambda_2 \\ \lambda_3 \end{bmatrix}$$

$$\pm\ indicates\ CCW - rotating\ or\ CW - rotating\ vectors\ respectively \quad (2.4)$$

$\hat{v}_o$ and $\hat{v}_i$ are the amplitudes of the output and input voltage vectors and $m = \frac{\hat{v}_o}{\hat{v}_i}$ is the modulation index. By solving the matrix equation (2.3) the duty ratios λ_1, λ_2 and λ_3 can be obtained for both the CCW rotating and CW rotating vectors. Moreover, the output voltage is calculated using (2.5). V^* is the output voltage.

$$V^* = \lambda_{1ccw}\vec{v}_{abc} + \lambda_{2ccw}\vec{v}_{bca} + \lambda_{3ccw}\vec{v}_{cab}\ (for\ CCW - rotating\ vectors)$$
$$V^* = \lambda_{1cw}\vec{v}_{acb} + \lambda_{2cw}\vec{v}_{cba} + \lambda_{3cw}\vec{v}_{bac}\ (for\ CW - rotating\ vectors) \quad (2.5)$$

The input grid power factor is affected by the type of rotating vectors chosen to modulate with. The use of CCW rotating vectors enables the drive to draw lagging currents from the grid whereas leading currents are drawn while CW rotating vectors are used. The power factor can be controlled by applying a combination of the CCW rotating and CW rotating vectors. The combination is determined by a ratio, x. The ratio is multiplied after the duty ratios are calculated using (2.3). An unity power factor is achieved by setting $x = 0.5$ and setting $x < 0.5$ gives a higher ratio of CW rotating vectors to be used hence drawing leading currents from the grid and a lagging power factor is obtained with $x > 0.5$.

The switching pulses are generated by comparing the aggregated duty ratios with a triangular carrier followed by logic computations. Figure 2.3 shows the generation of pulses using the aggregation of the duty ratios. (2.5) shows the aggregation of duty ratios produced by the CCW-rotating vectors and the CW-rotating vectors. The output pulses generated by the comparison of the aggregated duty ratios and the triangular carrier which are then NOR'd in the sequence shown in (2.6).

$$\Lambda_1 = x\lambda_{1ccw}$$

$$\Lambda_2 = x(\lambda_{1ccw} + \lambda_{2ccw})$$

$$\Lambda_3 = x(\lambda_{1ccw} + \lambda_{2ccw} + \lambda_{3ccw})$$

$$\Lambda_4 = x(\lambda_{1ccw} + \lambda_{2ccw} + \lambda_{3ccw}) + (1 - x)\lambda_{1cw}$$

$$\Lambda_5 = x(\lambda_{1ccw} + \lambda_{2ccw} + \lambda_{3ccw}) + (1 - x)(\lambda_{1cw} + \lambda_{2cw})$$

$$\Lambda_6 = x(\lambda_{1ccw} + \lambda_{2ccw} + \lambda_{3ccw}) + (1 - x)(\lambda_{1cw} + \lambda_{2cw} + \lambda_{3cw}) \quad (2.6)$$

$$P_1 = !\, p_1$$

$$P_2 = p_1 \oplus p_2$$

$$P_3 = p_2 \oplus p_3$$

$$P_4 = p_3 \oplus p_4$$

$$P_5 = p_4 \oplus p_5$$

$$P_6 = p_5 \oplus p_6 \quad (2.7)$$

Where, Λ_1 to Λ_6 are the aggregated duty ratios which are compared with the triangular carrier to produce the signals, p_1 to p_6. P_1 to P_6 are obtained by sequential NOR-ing of p_1 to p_6. The final switching pulses transmitted to the gate drivers are produced by combining P_1 to P_6 in different combinations for each corresponding phase.

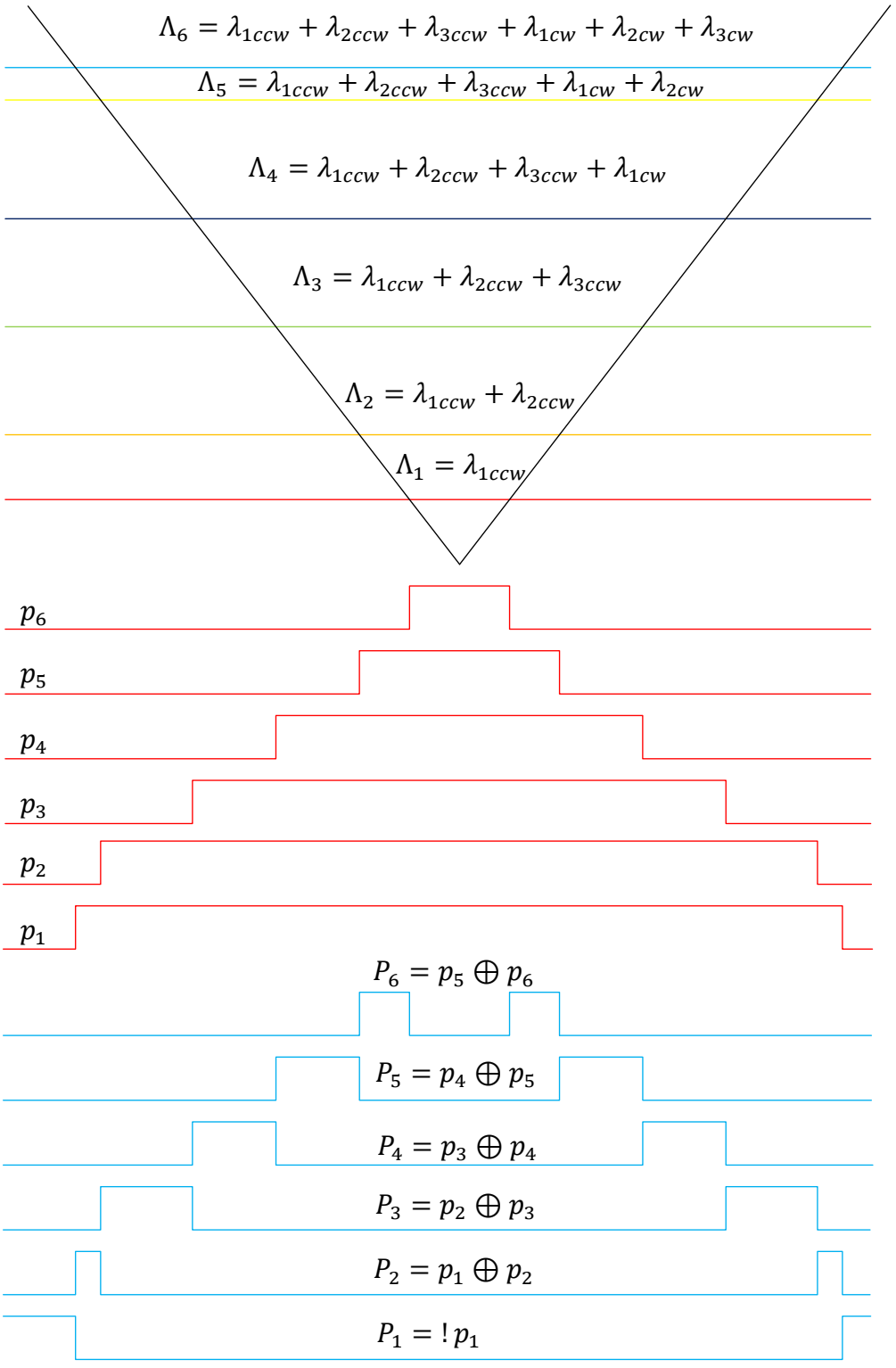

Fig 2.3 Generation of pulses using rotating vectors

2.2 Three level indirect matrix converter based open-end winding drive

The topology discussed in this section is a modification of the direct matrix converter drive topology, where the two direct matrix converters connected to the open-end winding motor are replaced with a front-end converter and two three-level inverters feeding the two ends. The front-end converter switches at a lower frequency and converts the input three-phase voltages into three-level voltages as max (V_{max}), mid (V_{mid}) and min (V_{min}). The three-level voltages are the inputs to the two three-level inverters, which feed three-phase voltages to the motor. The main advantages of this topology are:

- Lower switching frequency for the front end, which reduces switching losses
- No requirement of separate protection clamp circuit

The topology equips 36 switches in total with 12 switches for the front-end converter and 24 (2 x 12) switches for the two inverters. It has the same switch count as the direct matrix converter based open-end winding drive. The topology can be realized in two ways i.e., as a T-type converter drive as shown in Figure 2.4 or an I-type converter drive as shown in Figure 2.5. Both types have same count of switches but differ in terms of losses where T-type drive performs better due to lesser losses as discussed in [43]. The switches that connect the three-phase input voltages to the mid voltage (V_{mid}) bus are all four-quadrant switches since it requires bi-directional power flow capability and the other switches that connect to the max voltage (V_{max}) and min voltage (V_{min}) are two-quadrant. Individually, CONV, INV1 and INV2 are identical in terms of number of switches and configuration by each phase.

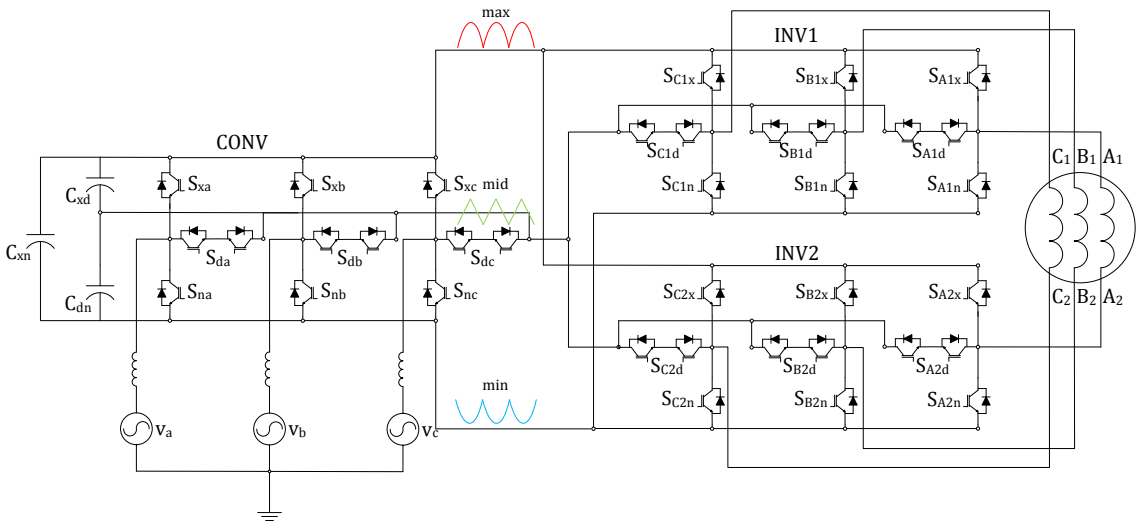

Fig 2.4 T-type indirect matrix converter based open-end winding drive

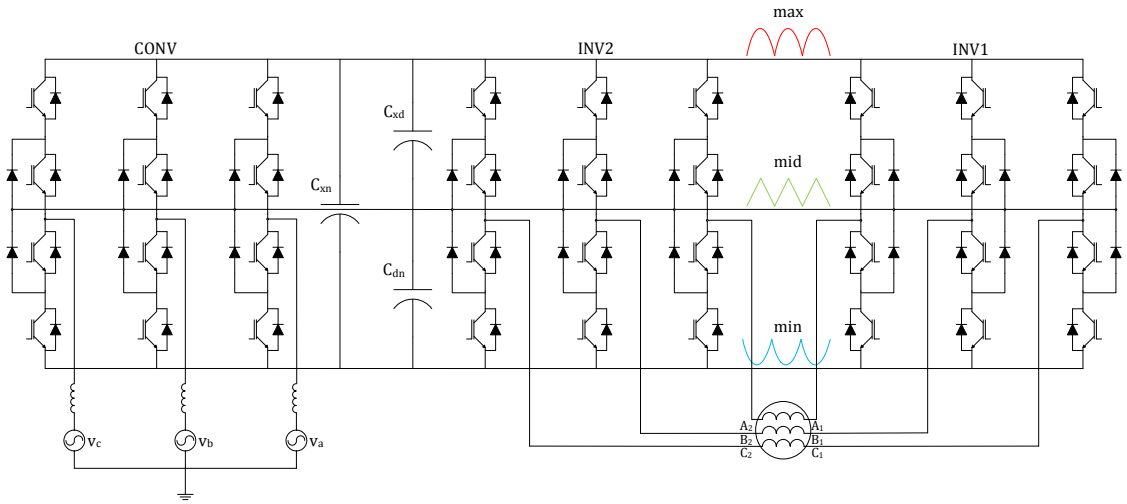

Fig 2.5 I-type indirect matrix converter based open-end winding drive

2.2.1 Indirect matrix converter – Switching and operation

The switching strategy for the converter can be separated into front-end converter switching and the inverter switching. As mentioned earlier, the switching frequency for the front-end converter is much lesser. The switching strategy for the inverters is similar to the one used for direct matrix converter based open-end winding drive.

2.2.1.1 Front end - Switching and operation

The front-end converter uses 12 switches with 4 in each leg. The switches connecting to the mid voltage bus are bi-directional and switch 6 times in a time period, T_s. The switches connecting to the max and min voltage buses switch 3 times in a time period. The strategy is to connect the highest phase from the input voltages to the V_{max} bus, lowest phase to the V_{min} bus and the other phase to the V_{mid} bus. The max voltage varies from $0.5 \times V_{ph_{peak}}$ to $V_{ph_{peak}}$ and mid varies from $-0.5 \times V_{ph_{peak}}$ to $0.5 \times V_{ph_{peak}}$ and min varies from $-V_{ph_{peak}}$to $-0.5 \times V_{ph_{peak}}$. The switching states for the converter are shown in Table 2.4. The three level voltages created by the converter is shown in Figure 2.6.

2.2.1.2 Three level inverter - Switching and operation

The operation of the inverters feeding the open-end winding is similar to the direct matrix converter for open-end winding. The power factor control described in section 2.2 is used here for switching of the inverters. From Table 2.1, in regions I, III and V, the converter produces positive sequence voltages and negative sequence voltages in the other three regions. The modulation method used in the grid power factor control where, the CCW-rotating and CW-rotating vectors are alternatively used is also used here to match the change in the phase sequences of the max, mid and min voltages. (2.6), (2.9) and (2.10) are used for the generation of duty ratios and the switching pulses with (2.7) and (2.8) being applied for control of grid power factor similarly. The primary difference in the switching strategy is that, the angle of rotation for the reference vector is $0\ to\ \pi/3\ to\ 0$ instead of $-\pi/2\ to\ \pi/2$ since the input to the inverters are the three-level voltages (max-mid-min).

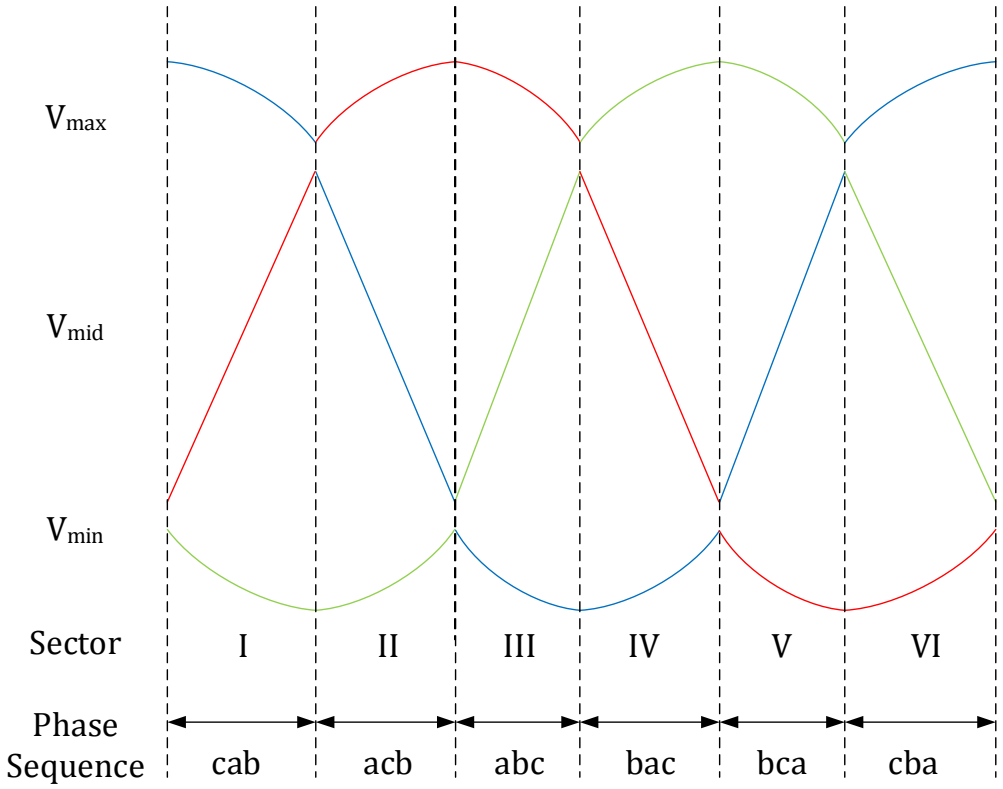

Fig 2.6 Three level (max-mid-min) voltages generated by the front-end converter

Region	v_{max}	v_{mid}	v_{min}	S_{ax} S_{bx} S_{cx}	S_{ad} S_{bd} S_{cd}	S_{an} S_{bn} S_{cn}
I	v_c	v_a	v_b	001	100	010
II	v_a	v_c	v_b	100	001	010
III	v_a	v_b	v_c	100	010	001
IV	v_b	v_a	v_c	010	100	001
V	v_b	v_c	v_a	010	001	100
VI	v_c	v_b	v_a	001	010	100

Table 2.1 Switching states for the front-end converter in each sector of the input voltage

2.3 Simulation of the drive with results and analysis

The indirect three-level matrix converter based open-end winding drive was modeled and simulated in Simulink/MATLAB using SimPowerSystems toolbox. The matrix converter was constructed using IGBTs with parallel diodes for the front-end converter and ideal switches for the two three-level inverters for faster simulation times. Ideal 208 V AC voltage sources were used to supply the drive. The open-end winding machine was mathematically modeled using a 3-phase, 60Hz, 208V, 4-pole induction motor model. The motor parameters for this model are given in Table 2.1. The inverters were switched at 10 kHz. The motor was operated at rated conditions using torque as input value for the load. The results for both the direct matrix converter based open-end winding drive and the three-level indirect matrix converter based drive are identical since the operation of both the drives are similar.

This drive model is also used to demonstrate the ride-through method, which is, discussed in Chapter 4. The simulation results are presented below.

Fig. 2.7 shows the max-mid-min voltages produced by the front-end converter. These voltages are hence used as input for the two three-level inverters to produce the open-end winding voltage. The open-end winding voltage across A_1A_2 is shown in Fig. 2.8. The open-end winding voltage being derived from the three-level voltages have the cup top waveform.

The motor phase currents and the input phase currents drawn from the grid are shown in Fig. 2.9 and Fig. 2.10 respectively. The motor phase currents are sinusoidal and the change in the magnitude is after the motor enters steady state after initial transients during motor startup. The input phase currents are nearly sinusoidal. The filter was designed to remove all the switching harmonics, although there is some presence of lower order harmonics, which are < 5% of the fundamental. In addition, the power factor control was tuned to obtain a unity power factor.

Finally, the common-mode voltage measured across the windings and the ground is shown in Fig. 2.11. It can be seen that the usage of rotating vectors for switching eliminates the common-mode voltage in the machine and hence reduces bearing currents.

Parameters	Value
Stator resistance (R_s)	1.77 Ω
Rotor Resistance (R_r)	1.34 Ω
Stator Leakage Reactance (X_{ls})	5.25 Ω
Rotor Leakage Reactance (X_{lr})	4.57 Ω
Mutual Reactance (X_m)	139 Ω
Moment of Inertia (J_{eq})	0.04 kgm^2
Slip (s)	0.0172

Table 2.2 Parameters of mathematical model of induction motor used in simulation

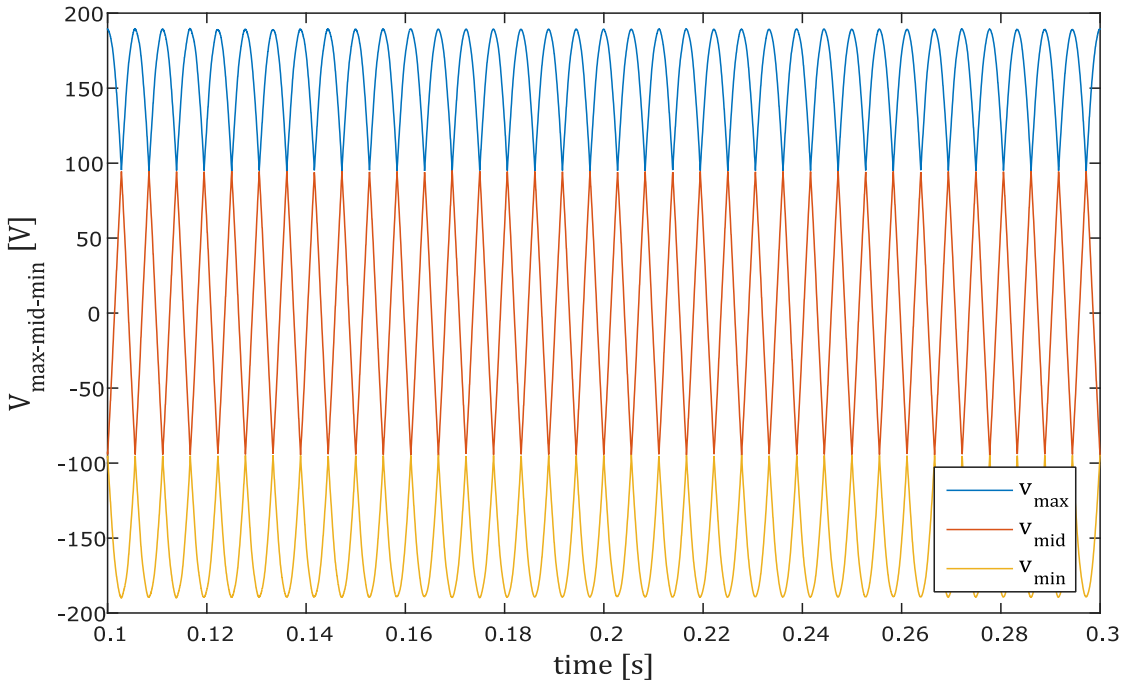

Fig 2.7 Max-mid-min voltages at the bus between the front-end converter and the inverters

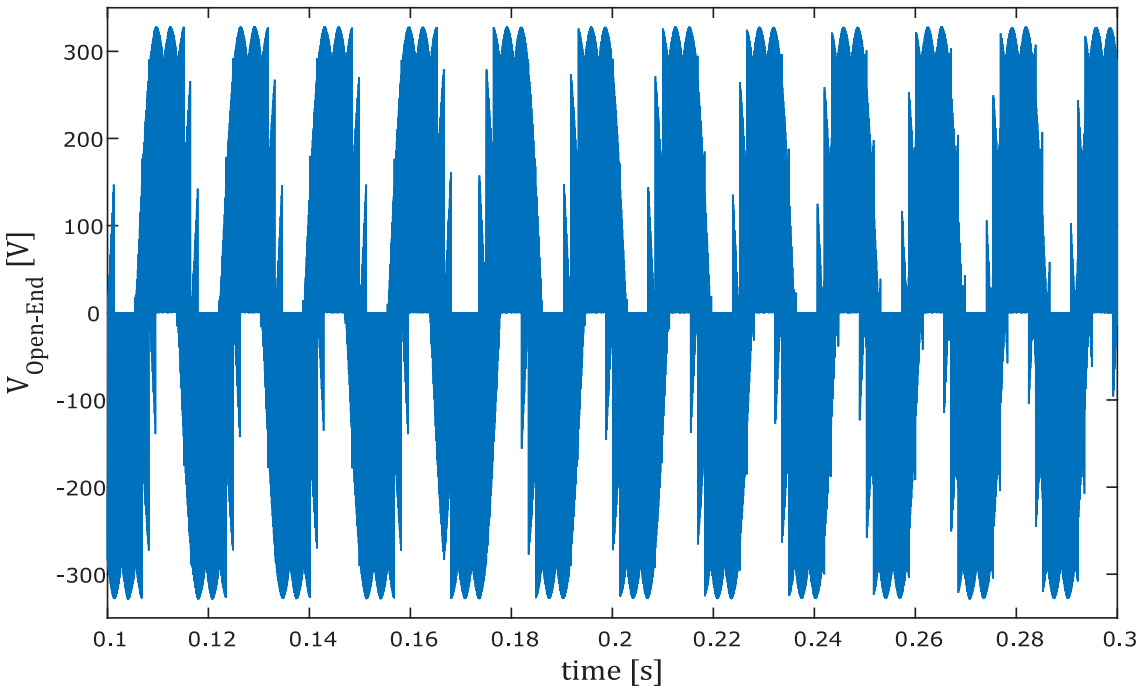

Fig 2.8 Open-end winding voltage across the terminals A1 and A2

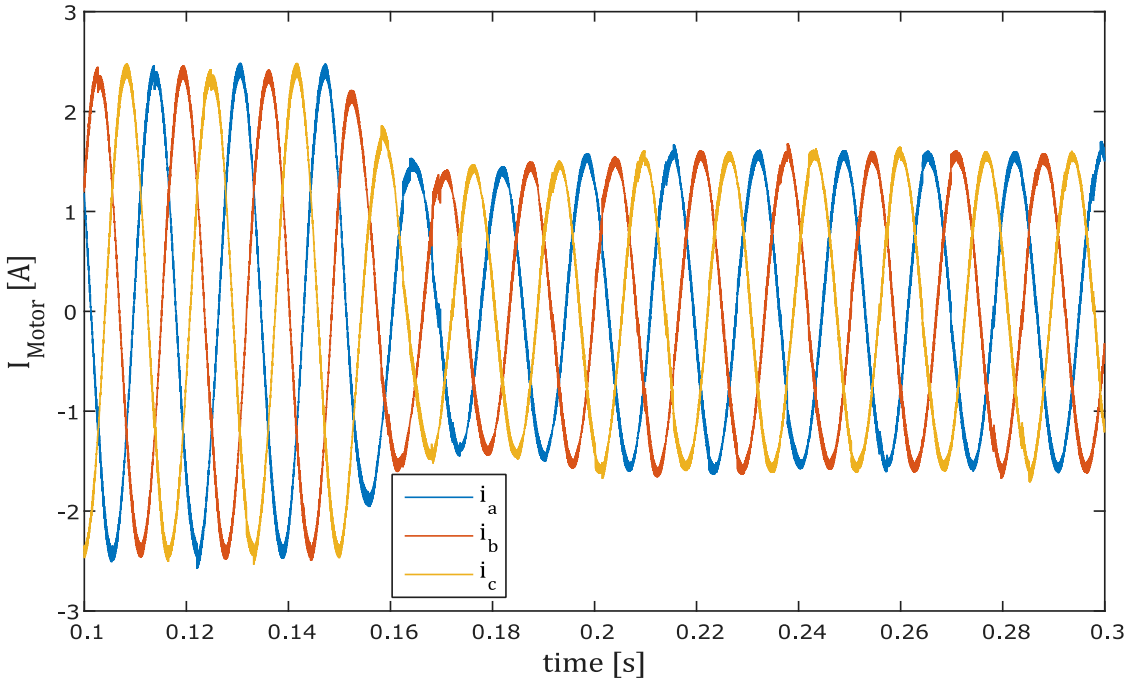

Fig 2.9 Three-phase currents through the motor terminals of the open-end winding machine

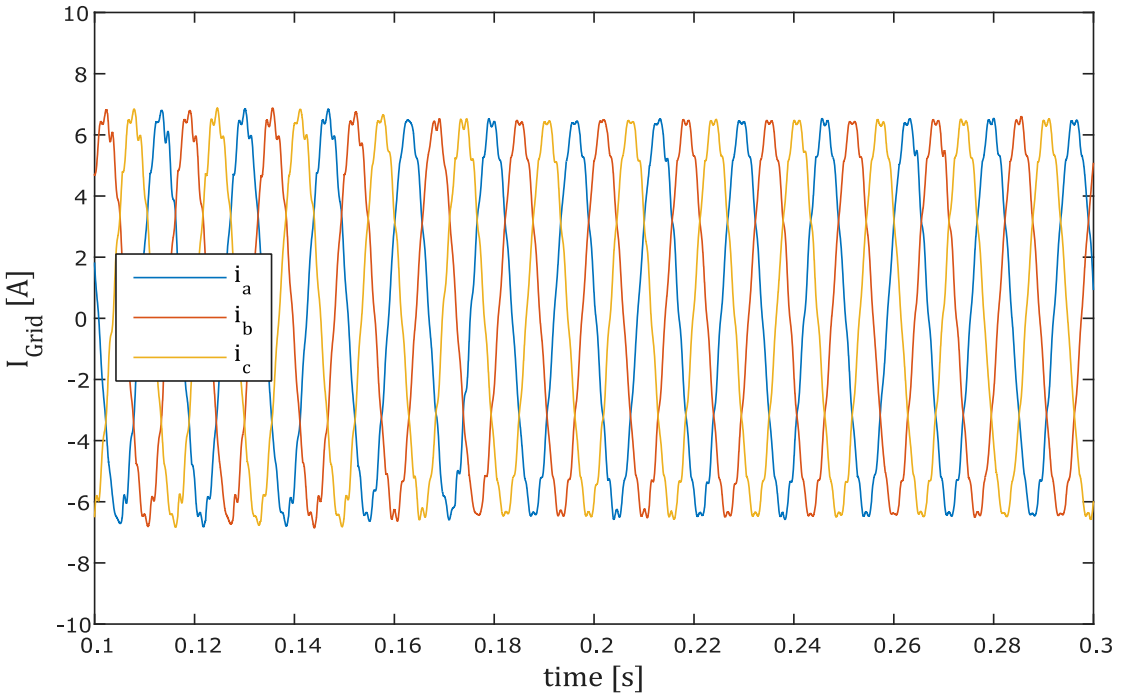

Fig 2.10 Input three-phase grid currents drawn by the open-end winding drive

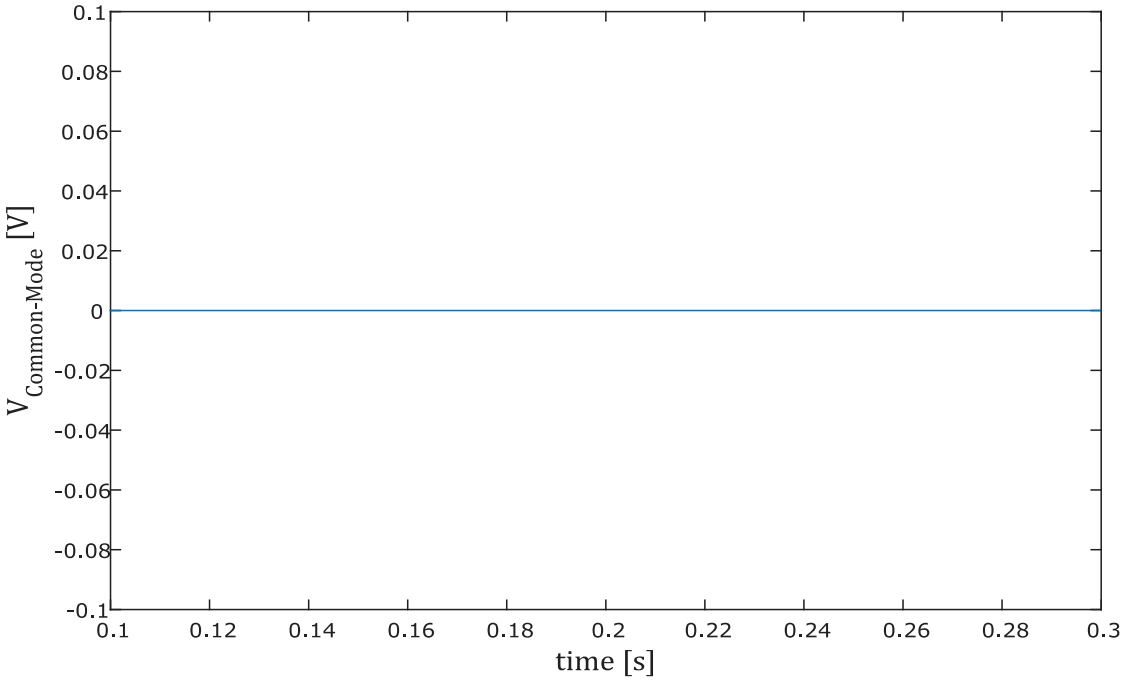

Fig 2.11 Common-mode voltage measured between the windings and the ground

2.4 Summary

This chapter presented a detailed description of a space-vector pulse width modulation method using only the rotating vectors from the set of 27 available vectors. The major advantage of using only rotating vectors is that at every time step, all three input phases are always connected to an output phase, which eliminates common mode voltage across the stator windings and the ground hence reducing bearing currents and the damage. Further, the application of the described pulse width modulation method for matrix converter based open-end winding drive was discussed. The theoretical modulation index limit while using rotating vectors is only 0.5. This is overcome by using two matrix converters to generate the output voltage, which increases the theoretical voltage ratio limit to 1.5.

The six rotating vectors comprise three counter-clockwise and three clockwise rotating vectors and they draw lagging and leading currents from the grid when used. Power factor control can be achieved by distributing the vectors accordingly to operate the drive in lagging, leading or unity power factor modes. The vectors are distributed by multiplying the generated duty ratios with a factor, x. In addition, the generation of voltages up to the 1.5 limit and the generation of pulses for both the converters using two complementary references are also presented.

Direct and indirect matrix converter based open-end winding drive topologies are described in detail. The direct drive comprises of two direct matrix converters and the indirect drive features a front-end converter generating three level (max-mid-min) voltages, which are fed to the two three-level inverters. The main advantages of the indirect drive over the direct drive are, reduced requirement for clamp circuit and lower losses due to lower switching frequency in the front-end converter. The indirect matrix converter is further outlined with details about the switching states of the front-end converter in every cycle of the input voltage. The drive was modeled in Simulink using switches from the simpowersystems blockset and the open-end winding induction motor was mathematically modeled. Simulation results were presented for a vector-controlled machine operated at rated conditions.

Chapter 3

Ride-Through method for Indirect Three-Level Matrix Converter based Open-End Winding Drive

This chapter proposes and describes a ride-through method for three-level indirect matrix converter based open-end winding drive that was presented in chapter three. The method uses the filter capacitor as an energy transfer mechanism from the motor-load inertia back to the motor to sustain the stator flux. This is achieved by using the filter capacitor as the new voltage source for the three-level inverters and the capacitor voltage is maintained using the energy from the inertia of the motor. The mechanism and the change in the control structure are explained in detail in the following subsections of the chapter. This ride-through strategy is easily implemented in the mentioned topology of matrix converter since the front-end naturally enables one to disconnect from the grid in the event of a fault.

The main advantages of the presented ride-through method are:

- Does not require additional energy storage devices to maintain the motor flux
- No modification of hardware or addition of extra semiconductor switches is required

3.1 System configuration during ride-through operation

During normal conditions, the three-level indirect matrix converter based open-end winding drive is operated in a configuration as shown in Fig. 3.1. The front-end converter produces three-level voltages (max-mid-min) from the input three-phase AC source and the two three-level inverters use the three-level voltages to produce AC voltage across the open-end winding of the machine.

When a grid fault occurs, the drive faces a voltage sag and is hence disconnected from the grid by switching off the IGBTs in the front-end converter. The switch states of the converters during the ride-through operation is shown in Fig 3.3. The front-end converter now operates like a three-phase diode bridge rectifier with back-to-back blocking diodes in the mid leg. The inverters operate with the same modulation as before and produces three-level output voltages. The system configuration during fault condition is shown in Fig 3.2. The filter capacitor (C_{fil} in Fig 3.2) act as the new voltage source for the inverters and the loop that controls the speed of the machine in a vector control scheme is changed to control the capacitor voltage. The strategy employed to use the filter capacitors as voltage sources for the inverters is presented in the next section.

3.2 Ride-Through strategy

Under normal operation, the drive transfers energy from the grid to supply the load (P_{load}); in addition, some energy is continuously lost in the electrical and mechanical systems (P_{losses}). Some energy is also stored in the rotational mass ($P_{kinetic}$) and the capacitor (P_{cap}) as shown in (3.1). The equation is written as a change in energy (ΔE) in (3.2). When a grid fault occurs, the drive is disconnected from the grid ($P_{grid} = 0$) as described in previous sub section and this is mathematically presented in (3.3). The rotational kinetic energy is recovered from the motor and the filter capacitor voltages are held at a higher level than grid voltages using the recovered energy. The capacitors are hence used as voltage sources for the two inverters, INV1 and INV2. Subsequently, they are operated as stand-alone three-level inverters and the reclaimed energy is used to supply E_{cap}, E_{load} and E_{losses} as shown in (3.4).

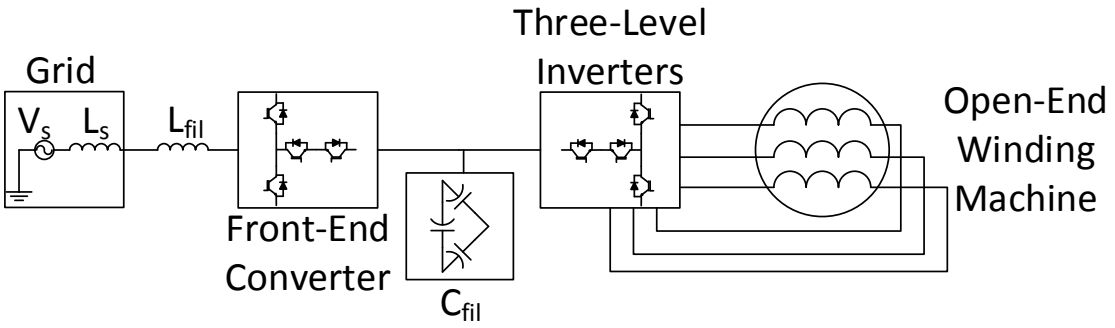

Fig 3.1 Drive configuration during normal operating conditions

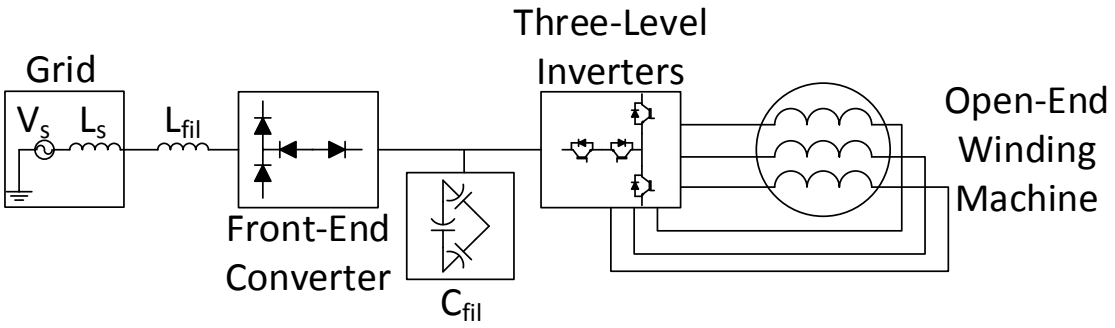

Fig 3.2 Drive configuration during ride-through operation

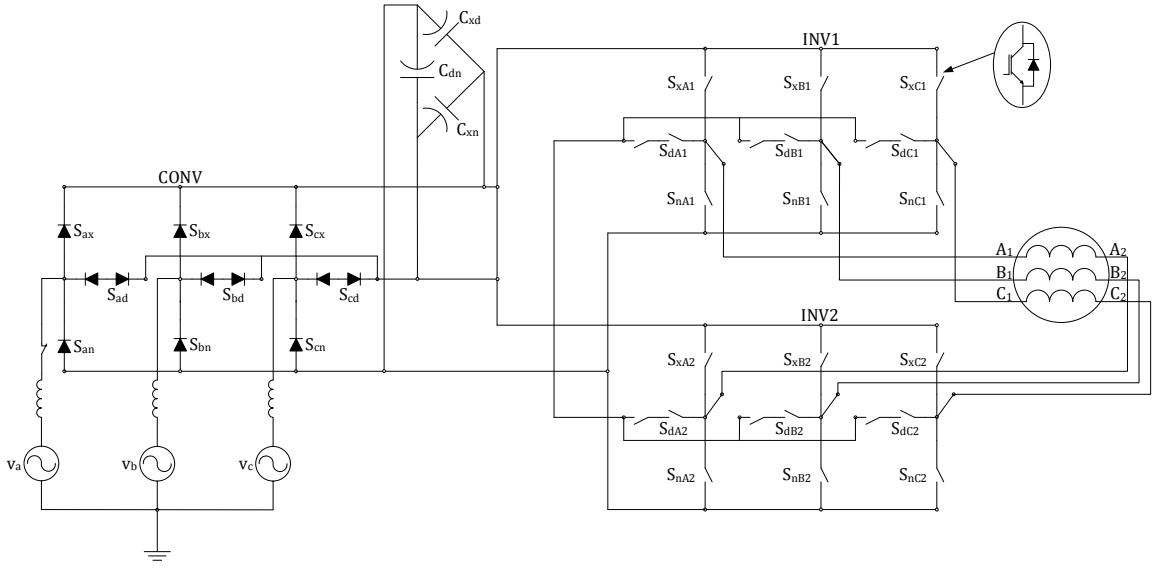

Fig 3.3 State of switches in the indirect matrix converter drive during ride-through operation

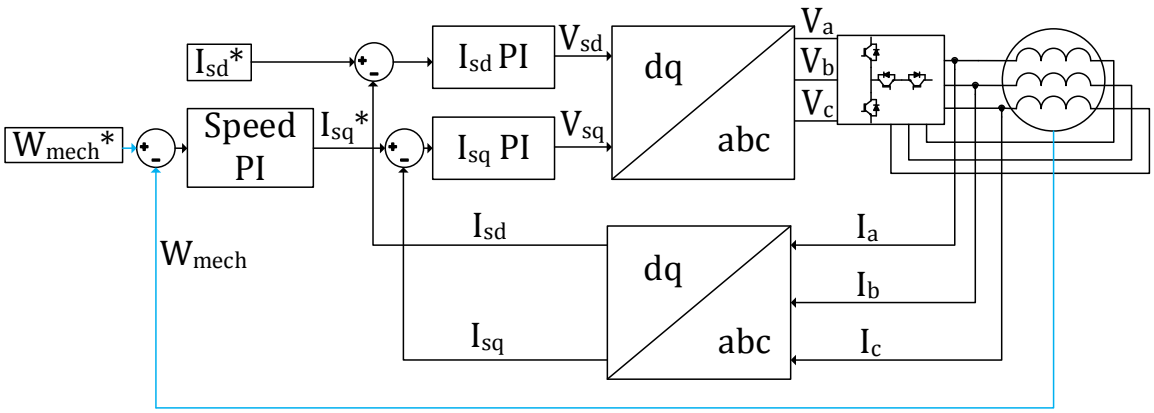

Fig 3.4 Control configuration during normal operation of the drive

$$P_{grid} = \mathrm{P_{cap}} + P_{kinetic} + P_{losses} + P_{load} \tag{3.1}$$

$$\Delta E_{grid} = \Delta E_{cap} + \Delta E_{kinetic} + \Delta E_{losses} + \Delta E_{load} \tag{3.2}$$

$$0 = \Delta E_{cap} + \Delta E_{kinetic} + \Delta E_{losses} + \Delta E_{load} \tag{3.3}$$

$$-\Delta E_{kinetic} = \Delta E_{cap} + \Delta E_{losses} + \Delta E_{load} \tag{3.4}$$

The energy transfer from the motor inertia to the capacitor is accomplished by modifying the vector control for ride-through operation during fault conditions. In normal operation, the flux is controlled by i_{sd} and the speed is controlled using i_{sq} as shown in Fig. 3.4. In the event of a grid fault, the loop controlling the flux is unaffected and the i_{sq} loop is changed to incorporate the control of the filter capacitor voltages by recovering the rotational kinetic energy from the motor, which is shown in Fig. 3.5. The system in (3.3) is expanded by replacing the ΔE terms with the corresponding expressions and is presented in (3.5). A small perturbation is added to the system to indicate the changes in the parameters during the fault. The perturbed system is shown in (3.6) as a small signal model. The terms, $\dot{V}_c^{\,*}$ and $\dot{\omega}_o$ are zero since they are differentials of constant values and $\widetilde{\Delta E}_{loss}$ and $\widetilde{\Delta E}_{load}$ are negligible. The simplified small signal model is shown in (3.7) where, $T\omega = \Delta E_{load} + \Delta E_{loss}$.

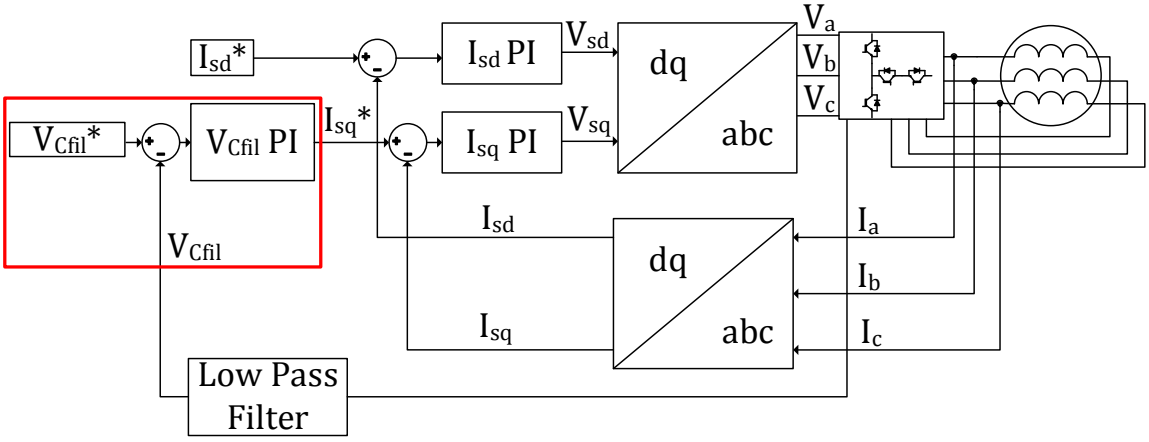

Fig 3.5 Control configuration during ride-through operation of the drive

$$0 = Cv_c\dot{v}_c + J\omega\dot{\omega} + \Delta E_{load} + \Delta E_{loss} \tag{3.5}$$

$$0 = C(v_c^* + \tilde{v_c})\left(\dot{v_c^*} + \dot{\tilde{v}_c}\right) + J(\omega_o + \tilde{\omega})\left(\dot{\omega_o} + \dot{\tilde{\omega}}\right) + \Delta E_{load} + \widetilde{\Delta E}_{load} + \Delta E_{loss} + \widetilde{\Delta E}_{loss} \tag{3.6}$$

$$0 = Cv_c^*\dot{\tilde{v}_C} + \omega(J\dot{\tilde{\omega}} + T) \tag{3.7}$$

Maintaining the capacitor voltage between max and min busses ($V_{C_{xn}}$) higher than the faulted input line voltage (which will be lower than normal voltage) makes sure that no power is drawn from the grid until the fault is cleared. Once the capacitor voltage is maintained at the desired level, the power drawn by the capacitor itself becomes negligible and all the energy is transferred to supply the losses and the load as shown in (3.8). Establishing the capacitor as an energy transfer device, we can equate the loss in kinetic energy to the energy in the capacitor, which is supplied to the load and the losses. (3.9) presents this in a mathematical form.

$$-\Delta E_{kinetic} = \Delta E_{losses} + \Delta E_{load} \tag{3.8}$$

$$\Delta E_{Cap} = \Delta E_{losses} + \Delta E_{load} = -\Delta E_{kinetic} \tag{3.9}$$

For designing a controller for the capacitor voltage loop a mathematical relation is established between the q-axis stator current (i_{sq}) and the capacitor voltage (V_c). The rotational kinetic energy is given in (3.10) and the power is obtained by differentiating it with respect to time as shown in (3.11). ω_o is the initial speed before the fault occurs and the speed at which the motor was operated in vector control. J is the moment of inertia and ω is the rotational speed of the motor.

$$E_{kinetic} = \frac{1}{2} J\omega^2 \tag{3.10}$$

$$P_{kinetic} = \frac{dE_{kinetic}}{dt} = J\omega_o \frac{d\omega}{dt} \tag{3.11}$$

$$P_{cap} = V_c^* I_c = V_c^* C \frac{dV_c}{dt} \tag{3.12}$$

The filter capacitor power is given by the product of its voltage and current (3.12) and $V_c^*$is the reference capacitor voltage. The filter capacitors are relatively smaller than the typical storage DC capacitors hence the control design is critical.

$$V_c^* C \frac{dV_c}{dt} = J\omega_o \frac{d\omega}{dt} \tag{3.13}$$

$$V_c^* C s V_c(s) = J\omega_o s\omega(s) \tag{3.14}$$

$$V_c(s) = \left(\frac{J}{CV_c^*}\omega_o\right)\omega(s) \tag{3.15}$$

$$V_c(s) = \frac{p}{2}\frac{L_m^2}{L_r}\, i_{sd}^* \frac{1}{sJ}\left(\frac{J\omega_o}{CV_c^*}\right) i_{sq}(s) \tag{3.16}$$

$$\frac{V_c(s)}{i_{sq}(s)} = \frac{p}{2}\frac{L_m^2}{L_r}\, \frac{i_{sd}^* \omega_o}{sCV_c^*} \tag{3.17}$$

Using (3.9), (3.11) and (3.12), the mathematical relation of energy transfer between the motor and the capacitor is established in (3.13). It is represented in the Laplace domain in (3.14) where, $V_c(s)$ is the capacitor voltage and $\omega(s)$ is the speed of the motor. (3.14) is rearranged to present the relation between $V_c(s)$ and $\omega(s)$ which is shown in (3.15). The rotational speed, $\omega(s)$ in (3.16) is substituted with equations from speed loop in vector

control during normal conditions to obtain (3.16) where, $i_{sq}(s)$ is the q-axis stator current, i_{sd} is the d-axis stator current, p is the number of poles and L_m and L_r are the magnetizing and rotor inductances.

The relation between $V_c(s)$ and $i_{sq}(s)$ is established in (3.17). A Proportional-Intergal controller for the loop is designed using the pole cancellation method with a phase margin of 60^o and a bandwidth of 125 rad/s (same as the speed loop).

3.3 Sequence of events in ride-through method

Among various types of faults, single-phase to ground faults are the most common and designing a solution for that covers 70 - 85% of the faults [44] in the power system as discussed in the previous chapter. The matrix converter drive sees the effect of the fault as a voltage sag in the faulty phase. Ride-through is implemented through a series of events starting with detection of fault using sequence components. Reduction in positive sequence component or the presence of zero/negative sequence components indicates the presence of a fault in that phase. In addition, a three-phase fault is detected by monitoring the input voltage magnitude and a reduction in it indicates a voltage sag/fault. It is followed by switching off the front-end converter to disconnect the system from the grid and replacement of the speed-control loop with the capacitor voltage control loop simultaneously. The capacitor voltage is hence maintained during ride-through using the energy transfer mechanism discussed in the previous section. The grid voltages are monitored continuously and after the fault clears, the front-end converter is switched on when the difference between the capacitor and the grid voltages is small so that the current transients are minimized. Finally, the filter capacitor voltage control loop is replaced with speed control loop and the reference speed is changed to a ramp to avoid a step change in the speed, which will require very high currents to be drawn from the input. The procedure is presented as a flow chart in Fig. 3.6.

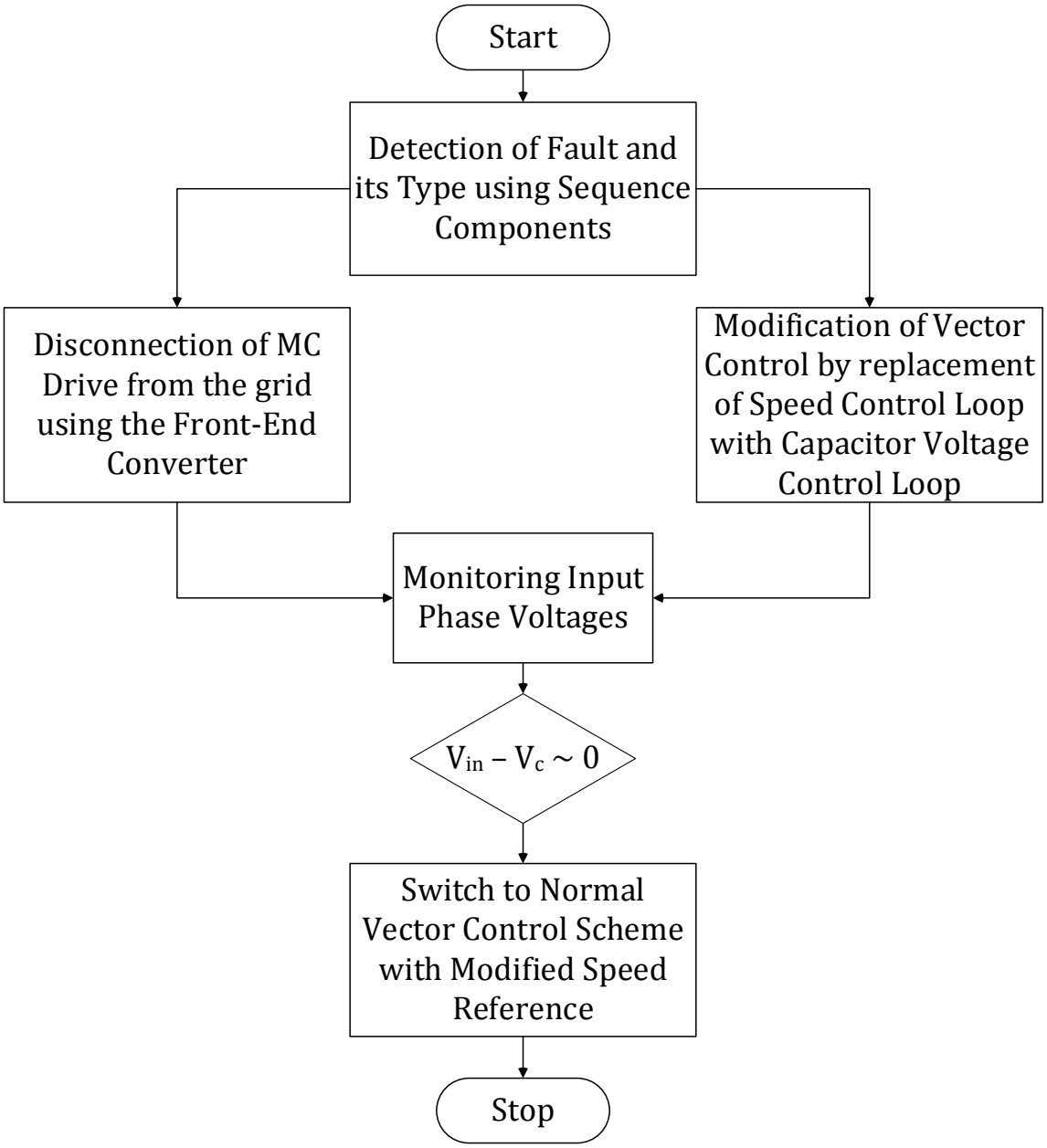

Fig 3.6 Sequence of events and procedure for the proposed ride-through method

3.4 System simulation with results and analysis

The three-level indirect matrix converter based open-end winding drive was modeled in Simulink/MATLAB using the SimPowerSystems toolbox set. The ride-through strategy was also implemented for the modeled system and was tested for a single-phase to ground fault and a three-phase to ground fault and the results were obtained. This section presents the system configuration used for modeling and the results of the simulation of the mentioned system with analysis. The drive configuration is same as mentioned in Chapter 2 during normal conditions. When a fault occurs, the fault is detected using sequence components in case of a single-phase to ground fault. The three-phase to ground fault detection was done by monitoring the magnitude of the input voltage and a drop in the magnitude indicates the presence of a fault. The implementation of this detection method for a single-phase fault is difficult due to the presence of a second harmonic waveform in the magnitude measurement when a fault occurs. Hence, the sequence components are used to detect a single-phase to ground fault. Both types of faults were simulated by reducing the magnitude(s) of the input source(s) since, when a grid fault occurs, the effect on the drive is essentially a sag in the input voltage.

3.4.1 Simulation of a single-phase to ground Fault

The system was simulated with a single-phase ground fault on the grid a-phase. The drive was disconnected from the grid by switching off all the IGBTs in the front-end converter and the drive was operated using the two three-level inverters with the input filter capacitor (C_{xn}) as the voltage source whose voltage is maintained by harvesting the kinetic energy from the motor.

A fault was simulated from 0.198s to 0.5s by creating a voltage sag to 0.5pu on phase-a (Adjustable speed drives are generally equipped to ride-through anywhere between 0.5 to 30 cycles). The following results were obtained. The grid-side results are presented first followed by the motor-side results. The filter capacitor voltages are shown in Fig. 3.7. During normal conditions, $V_{C_{xn}}$ vary from $V_{ph_{peak}}$ to $V_{L-L_{peak}}$ and $V_{C_{xd}}$ and $V_{C_{dn}}$ vary from 0 to $V_{ph_{peak}}$.

When the fault occurs, the modified control loop measures the actual $V_{C_{xn}}$ voltage and maintains it at the reference voltage of $V_{L-L_{peak}}$. It can be seen in the result that $V_{C_{xn}}$ stays at $V_{L-L_{peak}}$ throughout the duration of fault and $V_{C_{xd}}$ and $V_{C_{dn}}$ get balanced by the operation of the three-level inverters. This allows the capacitors to be the new voltage sources for the inverters during fault condition.

The grid phase voltages and the line voltages are shown in Fig. 3.8 and Fig. 3.9. The capacitor voltage, $V_{C_{xn}}$ is maintained higher than grid line voltage so that the front-end converter acts as a diode bridge and disconnects the drive from the grid. In Fig. 3.8, it can be seen that, due to the fault in phase-a, v_{ab} and v_{ca} sag and the other line voltage remains healthy. Similarly, v_a in Fig. sags to 0.5pu due to the fault in that phase as shown in Fig. 3.9.

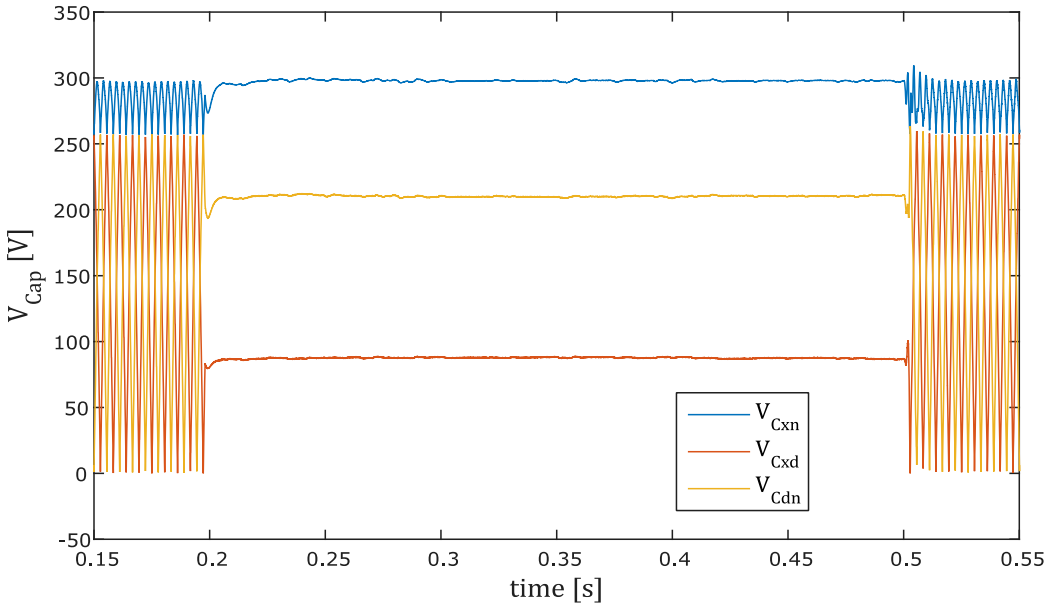

Fig 3.7 Filter capacitor voltages during normal and ride-through operations

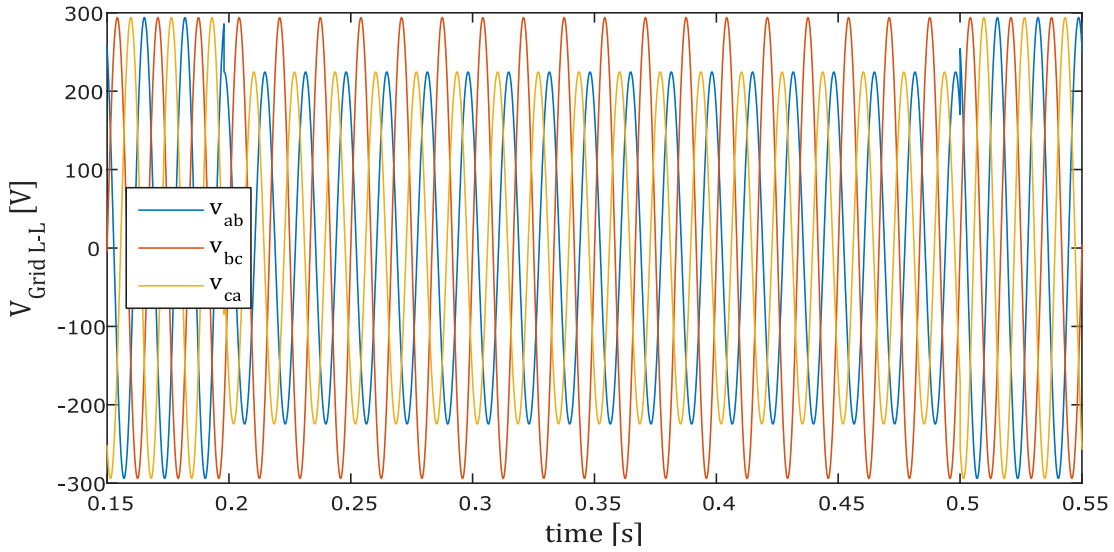

Fig 3.8 Grid line voltages during normal and ride-through operations

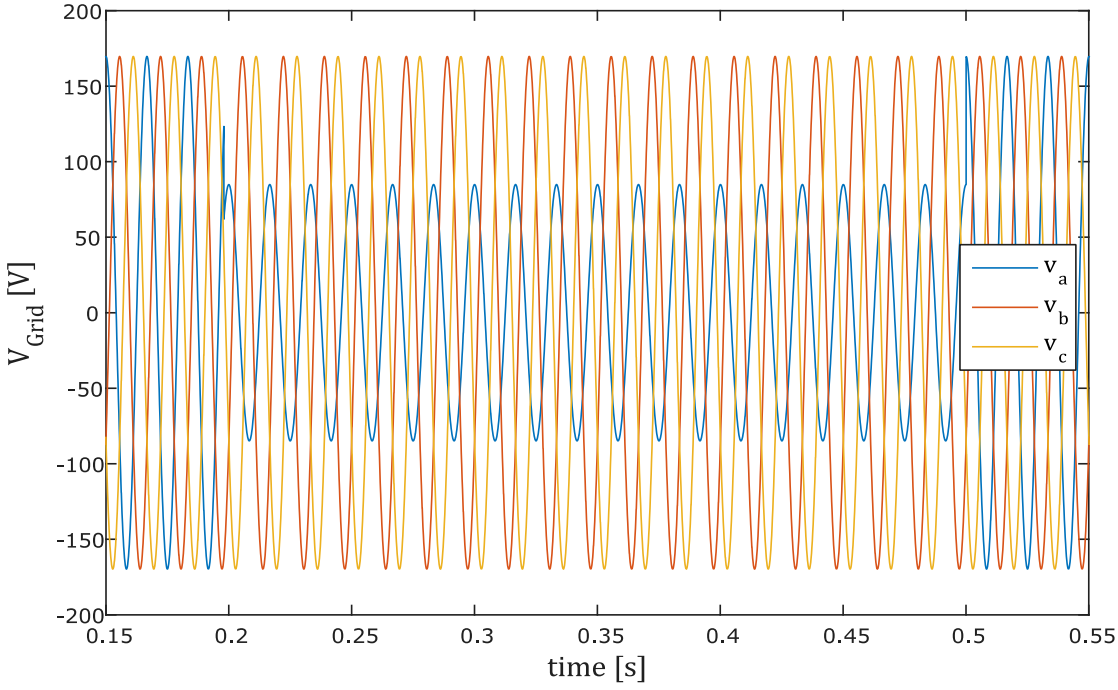

Fig 3.9 Grid phase voltages during normal and ride-through operations

Fig. 3.10 shows the input grid current drawn by the drive. During normal conditions, the currents are sinusoidal and when the fault occurs, they collapse to zero since the front-end converter disconnects the drive from the grid. After the fault is cleared, the drive is reconnected only if the difference between the capacitor voltages and the grid line voltages is < 5V. This makes sure that not huge currents are drawn from the grid once the drive starts to operate under normal conditions. The grid current shown in Fig. 3.10 does not have huge transients during reconnection but the small spike in the current peak is due to the motor's initial acceleration.

The open-end winding voltage across the winding A_1A_2 is shown in Fig. 3.11. The voltage waveform changes from a cup top to flattop during the ride-through operation. During normal operation, the open-end winding voltages are generated from the max-mid-min inputs which has the cup shaped waveform in v_{max} but when the fault occurs, the capacitors become the new voltage sources, which are constant and flat. Hence, the output voltage resembles the shape of a three-level waveform obtained from a typical three-level inverter.

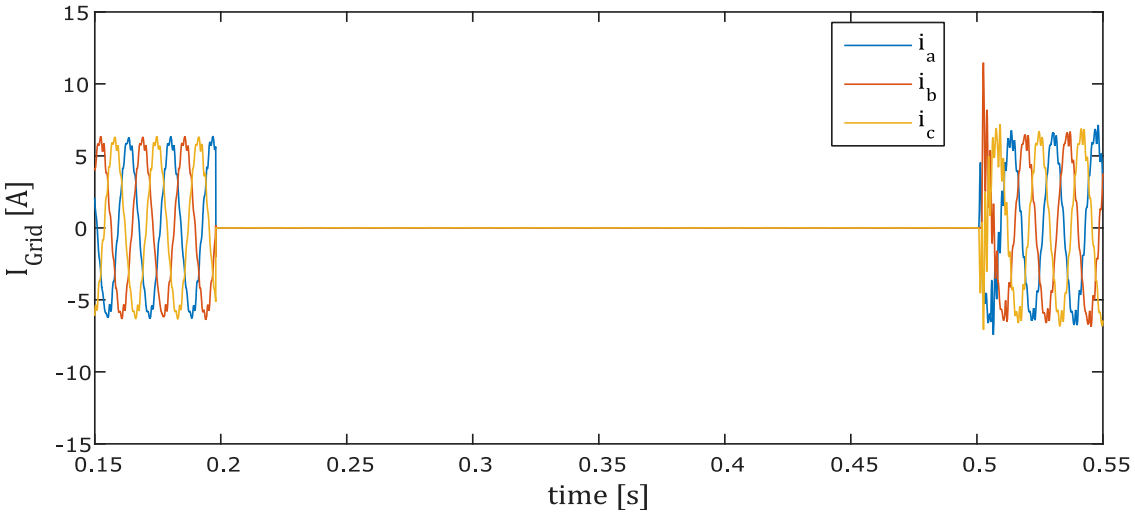

Fig 3.10 Grid currents during normal and ride-through operations

The motor dq-voltages are shown in Fig. 3.12. During the fault, v_{sq} reduces slightly since power is drawn from the motor to supply the losses and the flux in the motor. This is clearly indicated by the change in v_{sd} since the flux is controlled by the d-axis current and voltage. Once the fault clears the dq-voltages increase to supply the motor for re-acceleration and once the motor reaches the rated speed, the voltages settle to nominal values. The motor side results are presented on a longer time scale to accommodate the effects of motor transients.

Fig. 3.13 shows the motor dq-currents. The d-axis current, i_{sd} remains constant through the fault period, which shows that the stator flux does not drop during the ride-through operation, which is one of the primary requirements for any method. On the other hand, i_{sq} reduces to a value slightly negative. This is because the power is drawn from the motor to supply the losses and the motor flux. Once the drive reconnects to the grid, i_{sq} ramps up to 10 A to supply the motor acceleration. The current reduces to the normal value once the speed matches the reference.

The motor speed in rad/s is shown in Fig. 3.14. The motor is vector controlled during the normal operation and the speed is controlled to a reference of 185.25 rad/s (rated speed of the motor). During the ride-through operation, the speed control loop is replaced with the filter capacitor voltage control loop. With the capacitors supplying only the losses and flux of the motor and the kinetic energy being drawn from it, the speed of the motor drops. The rate of the speed drop depends on the motor inertia, J which is discussed in section 3.2.

After the drive reconnects, the control loops are restored to its original state and the motor is again in vector control. The speed reference is changed to ramp starting from the value it dropped to during the fault and saturates at the reference value. This is done to avoid the step change in the speed, which will cause huge transients in the current drawn from the grid.

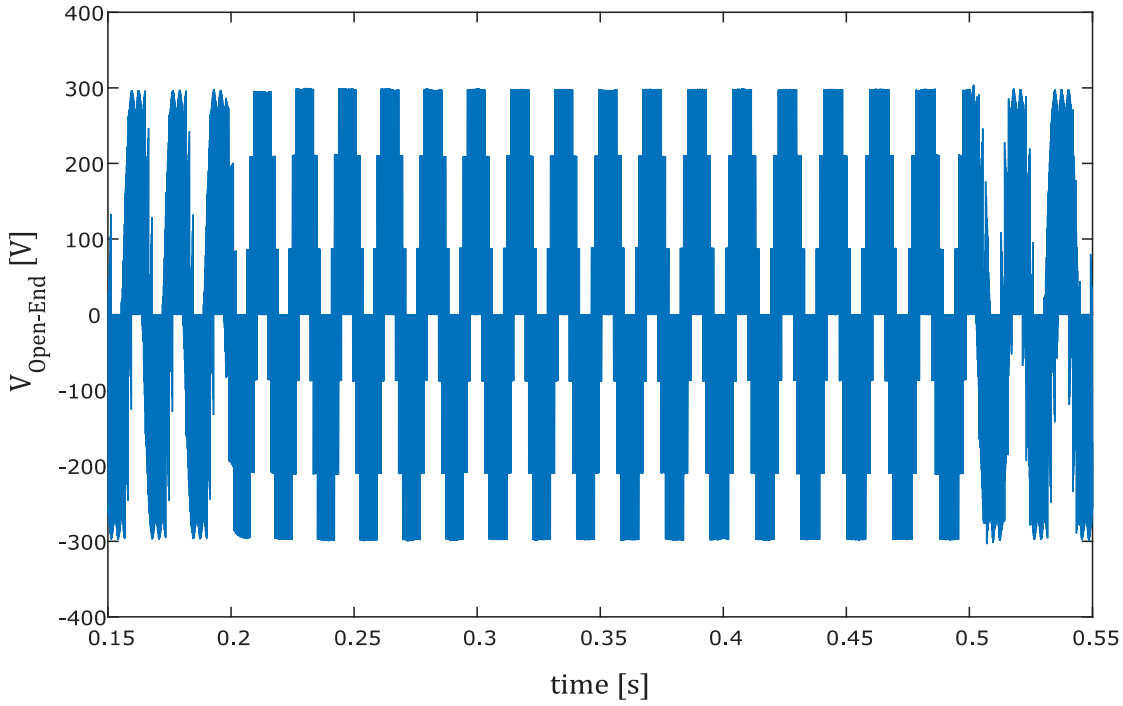

Fig 3.11 Open-end winding voltage during normal and ride-through operations

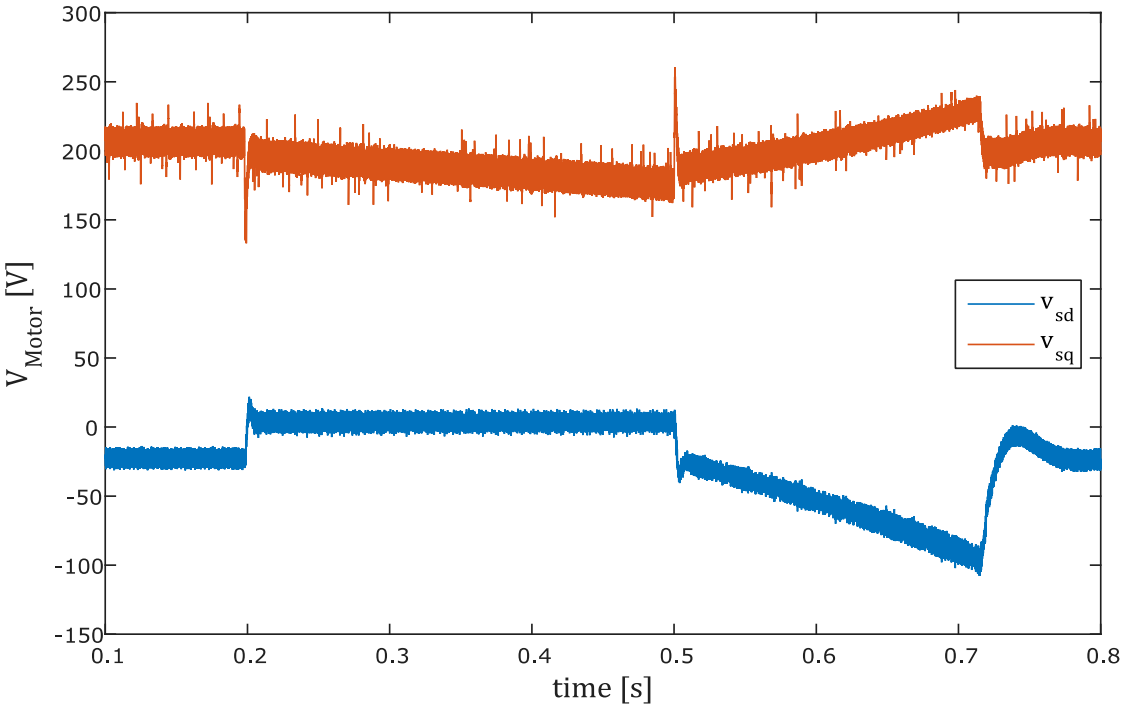

Fig 3.12 Motor dq-voltages during normal and ride-through operations

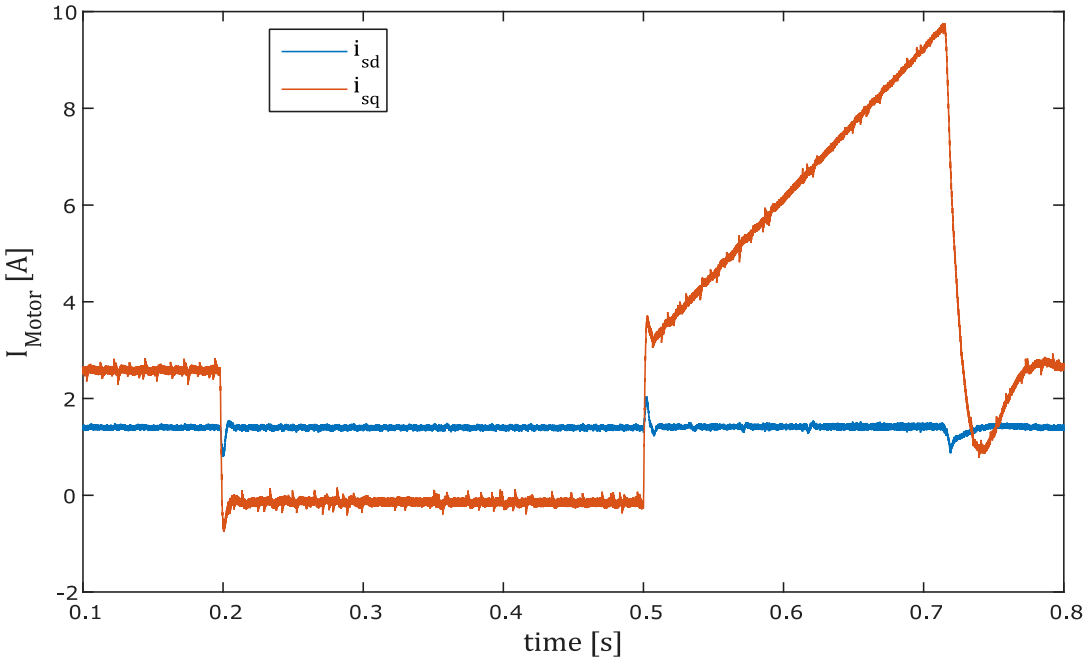

Fig 3.13 Motor dq-currents during normal and ride-through operations

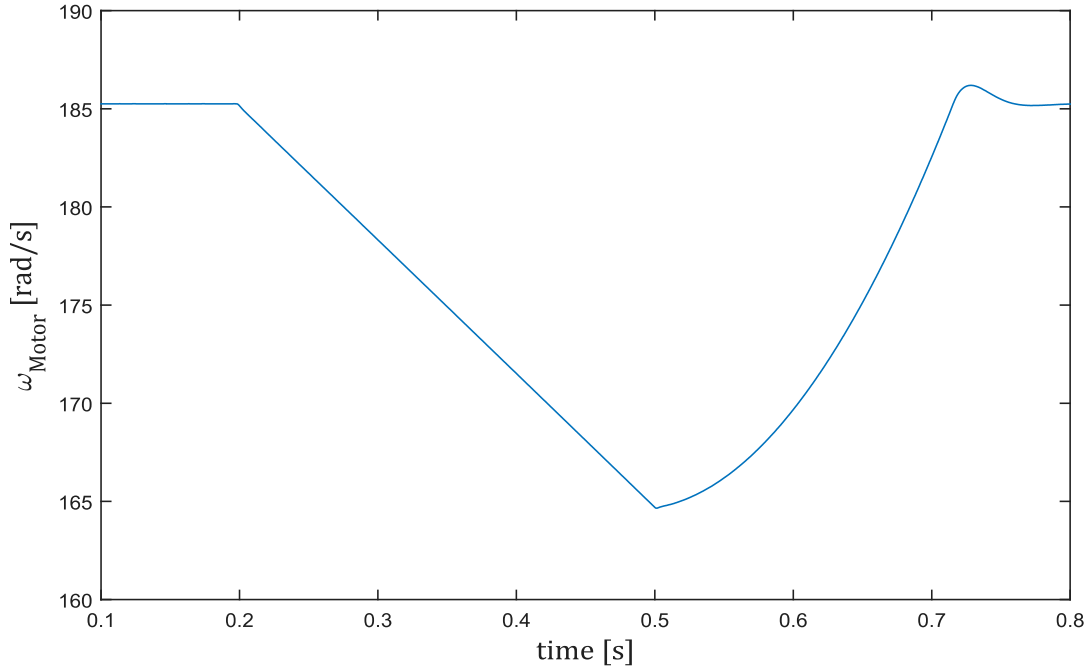

Fig 3.14 Motor speed during normal and ride-through operations

3.4.2 Simulation of a three-phase to ground fault

The system was also simulated to test the ride-through method for a three-phase to ground fault to cover its validity for majority of the faults in the system. A fault with a voltage sag to 0.5 pu in all three phases was created using the input voltage sources. The results are presented in Fig. 3.15. The grid side results are on the left: (top-bottom) capacitor voltage, grid line voltages, grid phase voltages and grid current. On the right hand side the motor side results are shown: (top-bottom): open-end winding voltage, motor dq-voltages, motor dq-currents and motor speed.

The results are similar to the ones obtained from the simulation of the system under a single-phase fault. The primary difference is the method of fault detection. The fault was detected by measuring the magnitude of the input voltage instead of using sequence components. In addition, since it is a three-phase fault, all the grid line and phase voltages reduce to 0.5 pu as shown in Fig. 3.15.

Grid side Results

Motor Side Results

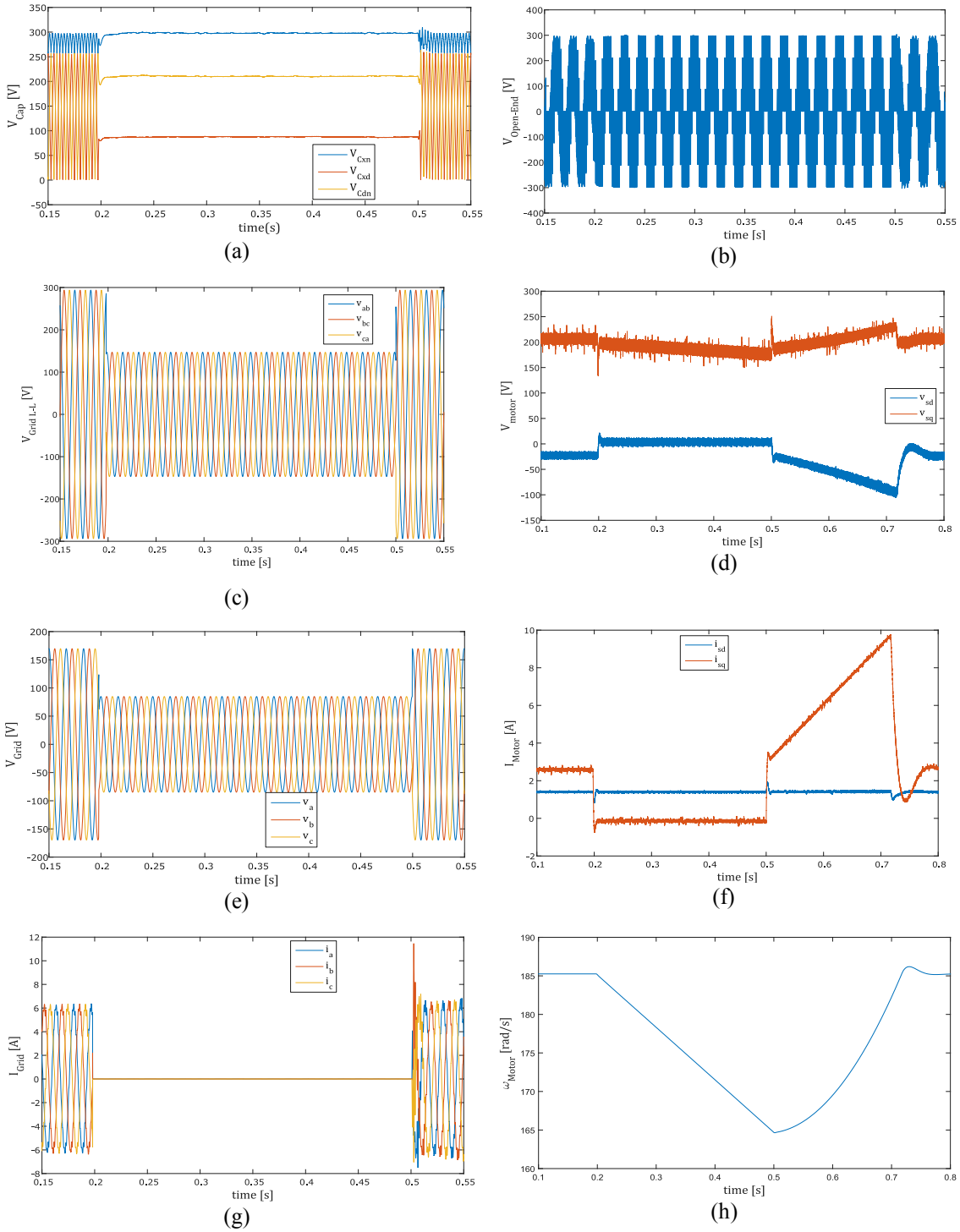

Fig 3.15 Simulation results for Three-Phase Fault: (a)Filter Capacitor Voltages, (b)Open-end winding voltages, (c)Grid line voltages, (d)Motor dq-voltages (e)Grid phase voltages, (f)Motor dq-currents, (g)Grid currents, (h)Motor speed

3.5 Experimental setup, analysis and results

For experimental verification, a two-level inverter based induction motor drive was built using Powerex PM50RL1A060 module. The drive control and the ride-through scheme was implemented using dSPACE DS1104 controller. The drive was supplied by a Hewlett-Packard 6010A DC power source. A $100\mu F$ capacitor was used on the DC bus, which acted as the voltage source during the fault condition. The fault in the system was created using a Gigavac DC Contactor controlled using a FET on the ISO1H811G Infineon board. The inverter drives a 230V, 1HP, 4-pole, 60Hz Baldor induction motor. It is mechanically coupled to a DC generator connected to a passive load. The induction motor parameters are shown in Table 3.1.

A detailed schematic of the experimental setup is shown in Fig. 3.16(c). During the ride-through operation, the indirect-matrix converter operates as a three-level inverter as described in Section 3.2. Hence, the proposed scheme is validated currently by implementing the method in a two-level inverter drive. During the fault condition, the filter capacitor on the DC bus acts the voltage source. The setup with labels is shown in Fig. 3.16(a) and 3.16(b). The results were obtained for two conditions:

i. DC generator is connected to a R load (R = 23.5Ω). A 190ms fault is created with ride-through disabled

ii. DC generator is connected to a RL load (R = 47Ω and L = $45mH$). A 250ms fault is created and ride-through is enabled

Both the tests were run using a 200V DC supply with the drive being speed controlled at 1000 rpm. Fig. 3.17 and Fig. 3.18, Fig. 3.19 show the results for conditions i, and ii respectively. Fig. 3.19 presents a detailed zoomed-in result for condition ii. The figures present the motor phase-a current, DC bus capacitor voltage, inverter phase-a voltage and input DC bus current from top to bottom as labeled. Fig. 3.20 shows the motor dq-voltages, motor dq-currents and the motor speed from top to bottom for the second condition.

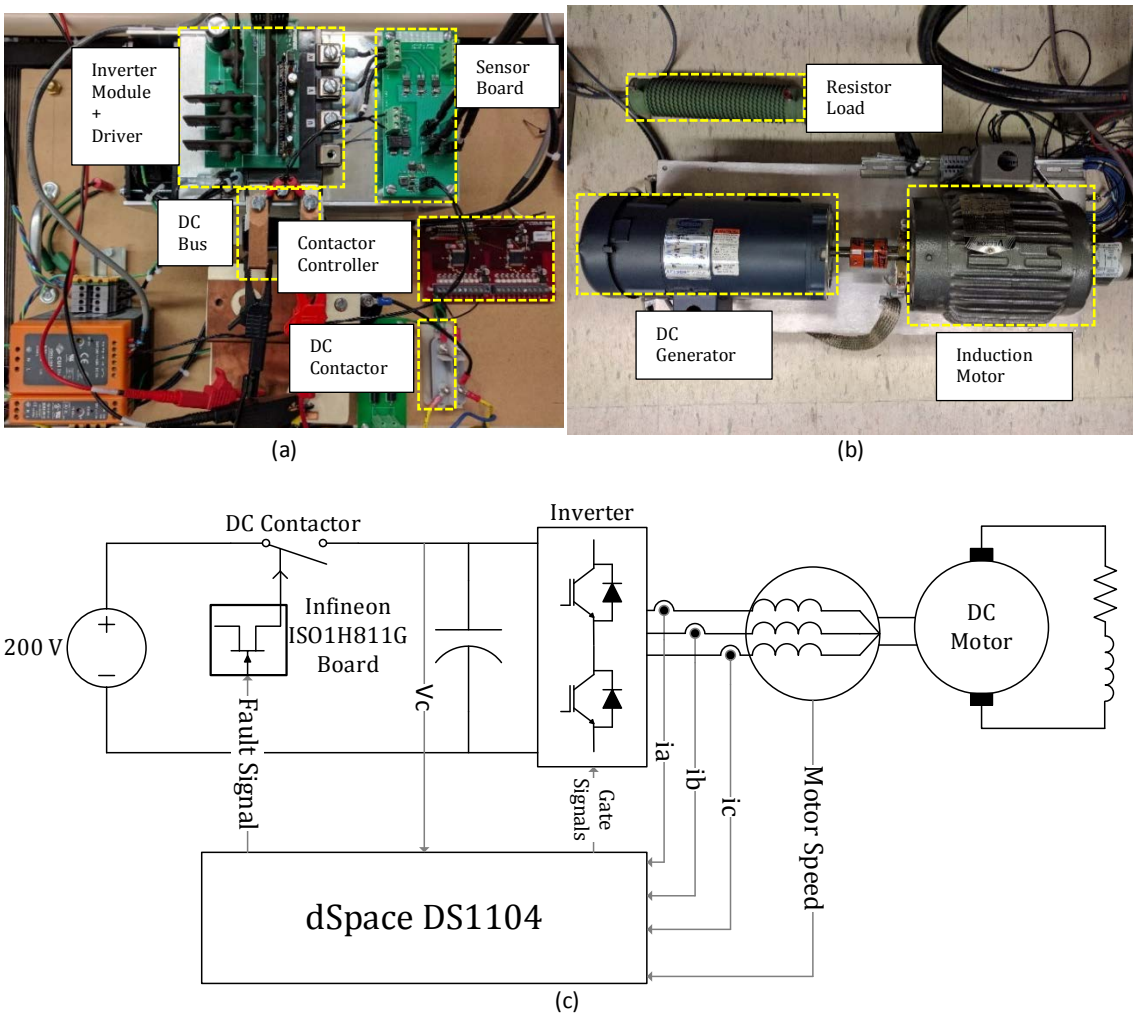

Fig 3.16 Experimental setup of the two-level inverter with DC Contactor, (b) Induction motor – DC generator pair with resistor load, (c) Schematic of the Experimental Setup

Parameters	Value
Stator resistance (R_s)	2.5 Ω
Rotor Resistance (R_r)	3.96 Ω
Stator Leakage Reactance (X_{ls})	2.37 Ω
Rotor Leakage Reactance (X_{lr})	3.55 Ω
Mutual Reactance (X_m)	85.99 Ω
Moment of Inertia (J_{eq})	0.0134 kgm^2
Slip (s)	0.0306

Table 3.1 Induction Motor Parameters

Results in Fig. 3.20 were plotted in Simulink using the data recorded from the Controldesk software. The test under the first condition is to demonstrate the operation of the drive in fault condition with ride-through disabled and present the detrimental effects of the fault on the drive itself.

Fig. 3.17 shows the collapse of the capacitor voltage (V_C) without the rotational kinetic energy being actively recovered from the motor. In addition, the inverter phase voltage (v_a) and the motor phase current (i_{motor}) indicate the loss in control of the motor since the frequency of both reduce significantly during the fault. During reconnection, the higher difference between the source voltage and the capacitor voltage causes a very high current to be drawn from the DC source (I_{in}), which forces the supply to enter constant current mode for a significant period. Subsequently, it creates an instability in the capacitor voltage, which is evident in the shown result.

The capacitor voltage (V_C) in Fig. 4.18 shows the apparent effect of enabling ride-through in the second test. The negative value of i_{sq} in Fig. 4.20 during the fault, indicates the energy recovery from the motor to maintain capacitor voltage. Hence, the motor speed reduces as the rotational kinetic energy falls. Moreover, i_{sd} remaining constant suggests that the flux in the motor is retained at the same value. During reconnection, the inrush in the input DC bus current is reduced as the difference between the capacitor voltage and the DC bus is low compared to the case without ride-through. I_{in} in Fig. 4.19 shows that the peak of the transient after the fault clears is less than two times the nominal value. The motor dq-voltages respond similar to the simulation results where, v_{sq} decreases during the fault and v_{sd} increases to small positive value and upon fault clear, both voltages recover to the pre-fault values after the motor re-accelerates to the reference value.

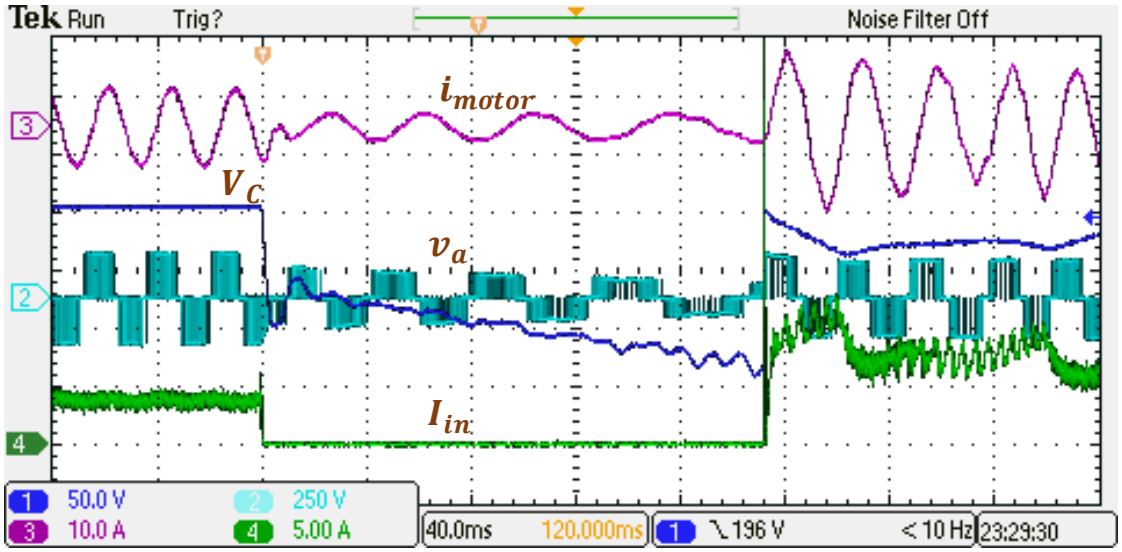

Fig 3.17 Experimental results for condition (i) when the drive was operated without ride-through enabled

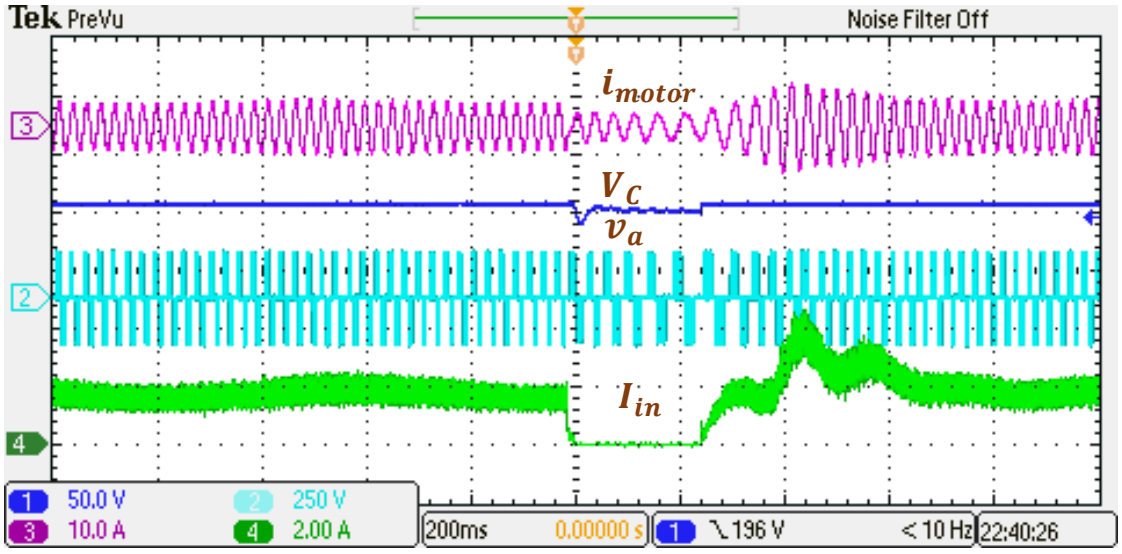

Fig 3.18 Experimental results for condition (ii) with ride-through enabled

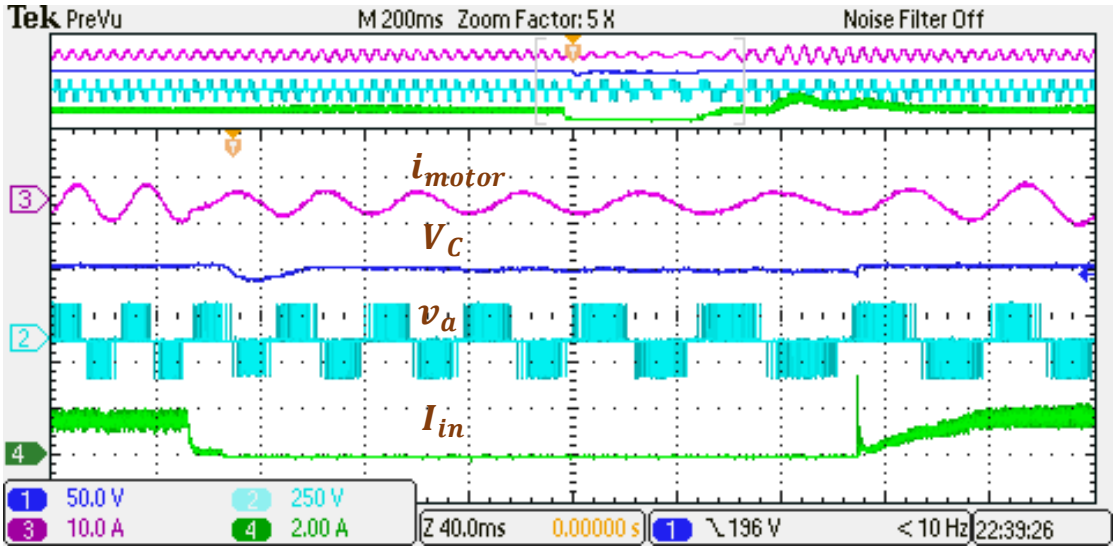

Fig 3.19 Detailed, zoomed-in (5x) Experimental results for condition (ii)

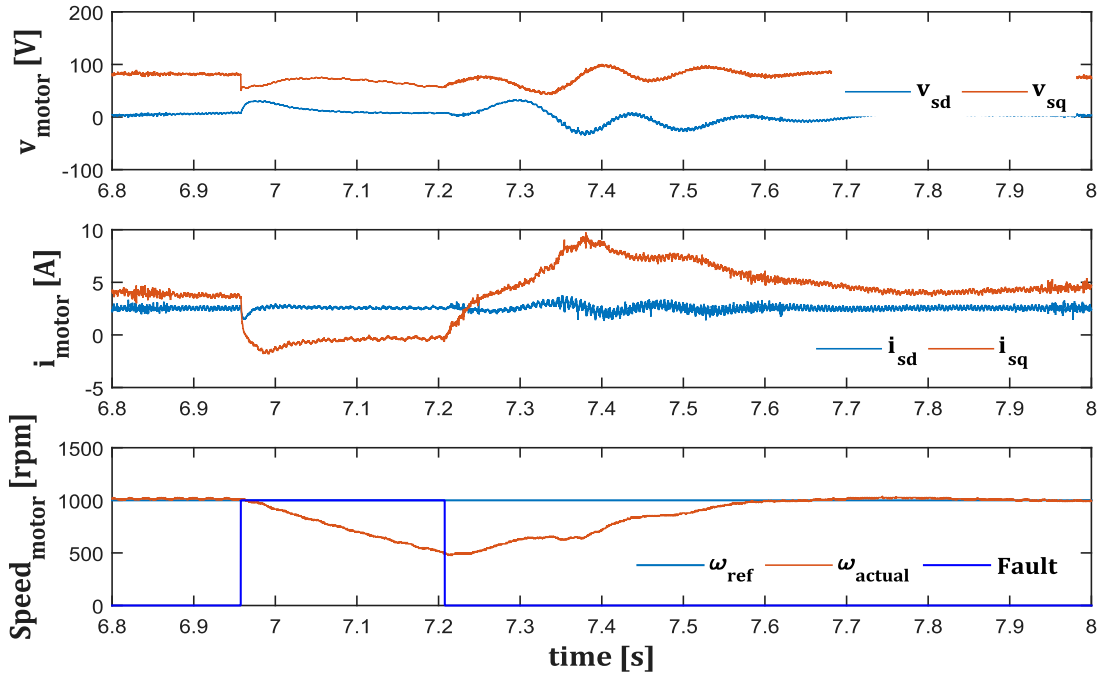

Fig 3.20 Motor dq-voltages, dq-currents and speed obtained from dSpace for ride-through operation under condition (ii)

3.6 Summary

A ride-through method using filter capacitors for the three-level indirect matrix converter based open-end winding drive was proposed. The strategy for the ride-through method was presented, where the kinetic energy from the motor is used during the ride-through operation to maintain the capacitor voltage and the capacitors are hence used as voltage sources for the two three-level inverters to supply the load and losses. The motor flux is also maintained this way.

During the ride-through operation, the control configuration is changed by replacing the speed control loop with a voltage control loop to maintain the capacitor voltage. A relation between $V_c(s)$ and $i_{sq}(s)$ was derived from the energy transfer equations and a PI controller was designed for the obtained transfer function. Further, the sequence of events during the ride-through operation was stated and discussed, where the drive is disconnected from the grid by switching off the front-end converter followed by replacement of the control loops, which enable the energy to be drawn from the motor and supplied back to maintain the flux and losses. When the fault clears, the drive is reconnected back to the grid when the difference between the grid line voltages and the capacitor voltages are significantly low. In addition, the speed reference is now changed to a ramp saturating at the previous reference value. These changes make sure that the input grid current transients are lowered.

The simulation results are presented for a single-phase fault and a three-phase fault created by causing a voltage sag in the input the voltage sources for 302 ms. The results corroborate the proposed method. Finally, an experimental setup using a two-level inverter is described and the results are provided for a fault of 250 ms. Since the matrix converter drive operates as inverter with the capacitor as voltage source during the fault, the experimental setup helps in verifying the proposed method.

Chapter 4

Conclusions and Future Work

4.1 Conclusions and summary

Ride-through solutions for matrix converters are essential for its commercialization and the proposed method offers a solution for operation of the drive during fault without additional storage devices or modification of the converter. Chapter 1 introduces the topics of adjustable speed drives, the types of faults and sags and the existing ride-through solutions available for the drives. The problem of common mode voltages in variable frequency drives is discussed and various solutions that address it are mentioned followed by the brief description of two types of matrix converter based open-end winding drives which eliminates the common mode voltages and provides a higher voltage gain depending on the application. The proposed ride-through method using the filter capacitors is briefly described and its advantages are mentioned.

Chapter 2 presents the space-vector pulse width modulation method using rotating vectors and explains in detail about the advantages (elimination of common-mode voltage) and limitations (lower voltage ratio) over using stationary vectors. Two matrix converter topologies for the open-end winding drive are described, including a direct and a three-level indirect matrix converter configuration. The indirect matrix converter drive have two primary advantages over the direct drive: reduced clamp circuit requirement and lower switching losses. In addition, it provides a convenient gateway to implement the proposed ride-through strategy without any modifications to the topology. The application of these vectors for the matrix converter based open-end winding drives are presented. The system was modeled in Simulink with a mathematical induction motor model and results are presented for operation of the drive in rated conditions under vector control. The results validate the advantages of matrix converter based open-end winding drive by demonstrating the elimination of common-mode voltages.

Chapter 3 proposes the ride-through strategy for the indirect matrix converter drive and presents the strategy used in its implementation: transfer of kinetic energy from the motor during the grid fault to supply the losses and maintain the flux by using the filter capacitors as the voltage source for the three-level inverters. The sequence of events in the implementation of the ride-through method starting with the disconnection of the drive from the grid followed by the change of control loops in the vector control scheme to control the capacitor voltage is described. Simulation results using the system model in Simulink are presented for a single-phase and a three-phase fault causing voltage sag up to 0.5 pu. The results verify the functioning of the proposed method and demonstrate the advantage of using the indirect topology as no modifications in the system was necessary. An experimental setup was built using a two-level inverter and the ride-through scheme was implemented in it to validate it. The results demonstrated the effectiveness of the method in maintaining the motor flux and elimination of transients during reconnection.

4.2 Future work

The discussed indirect matrix converter drive for open-end winding machines are highly advantageous over its predecessors and investigation of following ideas will aid in its commercialization:

- Implementation of a ride-through strategy for the generation mode operation of the open-end winding drive: The indirect nature of the topology allows the three-level inverters to operate independent of input grid voltages since their references for operation (modulation) are the three (max-mid-min) level voltages. Upon establishment of the three-level voltages, the front-end could be operated as a three-level inverter with the new reference from the input grid voltage during the fault. This implementation will be useful for the application of the drive in wind turbines.
- Operation of the indirect matrix converter under unbalanced voltage conditions
- Direct torque control of open-end winding induction motors using indirect matrix converter

References

1. C. Klumpner, M. Liserre and F. Blaabjerg, "Improved control of an active-front-end adjustable speed drive with a small de-link capacitor under real grid conditions," 2004 IEEE 35th Annual Power Electronics Specialists Conference (IEEE Cat. No.04CH37551), 2004, pp. 1156-1162 Vol.2.
2. T. Friedli, J. W. Kolar, J. Rodriguez and P. W. Wheeler, "Comparative Evaluation of Three-Phase AC–AC Matrix Converter and Voltage DC-Link Back-to-Back Converter Systems," in IEEE Transactions on Industrial Electronics, vol. 59, no. 12, pp. 4487-4510, Dec. 2012.
3. S. Yang, A. Bryant, P. Mawby, D. Xiang, L. Ran and P. Tavner, "An Industry-Based Survey of Reliability in Power Electronic Converters," in IEEE Transactions on Industry Applications, vol. 47, no. 3, pp. 1441-1451, May-June 2011.
4. J. W. Kolar et al., "PWM Converter Power Density Barriers," 2007 Power Conversion Conference - Nagoya, Nagoya, 2007, pp. P-9-P-29.
5. M. Venturini and A. Alesina, "The generalised transformer: A new bidirectional, sinusoidal waveform frequency converter with continuously adjustable input power factor," 1980 IEEE Power Electronics Specialists Conference, Atlanta, Georgia, USA, 1980, pp. 242-252.
6. Lixiang Wei, T. A. Lipo and Ho Chan, "Matrix converter topologies with reduced number of switches," 2002 IEEE 33rd Annual IEEE Power Electronics Specialists Conference. Proceedings (Cat. No.02CH37289), 2002, pp. 57-63 vol.1.
7. J. W. Kolar, M. Baumann, F. Schafmeister and H. Ertl, "Novel three-phase AC-DC-AC sparse matrix converter," APEC. Seventeenth Annual IEEE Applied Power Electronics Conference and Exposition (Cat. No.02CH37335), Dallas, TX, 2002, pp. 777-791 vol.2.

8. S. Raju and N. Mohan, "Indirect three level matrix converter," 7th IET International Conference on Power Electronics, Machines and Drives (PEMD 2014), Manchester, 2014, pp. 1-6.

9. T. Satish, K. K. Mohapatra and N. Mohan, "Modulation methods based on a novel carrier-based PWM scheme for matrix converter operation under unbalanced input voltages," Twenty-First Annual IEEE Applied Power Electronics Conference and Exposition, 2006. APEC '06., Dallas, TX, 2006, pp. 6 pp.-.

10. Y. d. Yoon and S. k. Sul, "Carrier-Based Modulation Technique for Matrix Converter," in IEEE Transactions on Power Electronics, vol. 21, no. 6, pp. 1691-1703, Nov. 2006.

11. D. Casadei, G. Serra, A. Tani and L. Zarri, "Matrix converter modulation strategies: a new general approach based on space-vector representation of the switch state," in IEEE Transactions on Industrial Electronics, vol. 49, no. 2, pp. 370-381, Apr 2002.

12. Han Ju Cha and P. N. Enjeti, "An approach to reduce common-mode voltage in matrix converter," in IEEE Transactions on Industry Applications, vol. 39, no. 4, pp. 1151-1159, July-Aug. 2003.

13. L. Huber and D. Borojevic, "Space vector modulated three-phase to three-phase matrix converter with input power factor correction," in IEEE Transactions on Industry Applications, vol. 31, no. 6, pp. 1234-1246, Nov/Dec 1995.

14. S. H. Hosseini and E. Babaei, "A new generalized direct matrix converter," ISIE 2001. 2001 IEEE International Symposium on Industrial Electronics Proceedings (Cat. No.01TH8570), Pusan, 2001, pp. 1071-1076 vol.2.

15. B. Ge, Q. Lei, W. Qian and F. Z. Peng, "A Family of Z-Source Matrix Converters," in IEEE Transactions on Industrial Electronics, vol. 59, no. 1, pp. 35-46, Jan. 2012.

16. C. Rojas et al., "Predictive control of a direct matrix converter operating under an unbalanced AC source," 2010 IEEE International Symposium on Industrial Electronics, Bari, 2010, pp. 3159-3164.

17. P. W. Wheeler, J. Rodriguez, J. C. Clare, L. Empringham and A. Weinstein, "Matrix converters: a technology review," in IEEE Transactions on Industrial Electronics, vol. 49, no. 2, pp. 276-288, Apr 2002.

18. S. Ogasawara, H. Ayano and H. Akagi, "An active circuit for cancellation of common-mode voltage generated by a PWM inverter," PESC97. Record 28th Annual IEEE Power Electronics Specialists Conference. Formerly Power Conditioning Specialists Conference 1970-71. Power Processing and Electronic Specialists Conference 1972, St. Louis, MO, 1997, pp. 1547-1553 vol.2.

19. K. Euerle, K. Iyer, E. Severson, R. Baranwal, S. Tewari and N. Mohan, "A compact active filter to eliminate common-mode voltage in a SiC-based motor drive," 2016 IEEE Energy Conversion Congress and Exposition (ECCE), Milwaukee, WI, 2016, pp. 1-8.

20. A. L. Julian, G. Oriti and T. A. Lipo, "Elimination of common-mode voltage in three-phase sinusoidal power converters," in IEEE Transactions on Power Electronics, vol. 14, no. 5, pp. 982-989, Sep 1999.

21. K. Basu, A. C. Umarikar, K. K. Mohapatra and N. Mohan, "High-frequency transformer-link three-level inverter drive with common-mode voltage elimination," 2008 IEEE Power Electronics Specialists Conference, Rhodes, 2008, pp. 4413-4418.

22. Yen-Shin Lai and Fu-San Shyu, "Optimal common-mode Voltage reduction PWM technique for inverter control with consideration of the dead-time effects-part I: basic development," in IEEE Transactions on Industry Applications, vol. 40, no. 6, pp. 1605-1612, Nov.-Dec. 2004.

23. Hee-Jung Kim, Hyeoun-Dong Lee and Seung-Ki Sul, "A new PWM strategy for common-mode voltage reduction in neutral-point-clamped inverter-fed AC motor drives," in IEEE Transactions on Industry Applications, vol. 37, no. 6, pp. 1840-1845, Nov/Dec 2001.

24. K. K. Mohapatra and N. Mohan, "Open-End Winding Induction Motor Driven With Matrix Converter For Common-Mode Elimination," 2006 International Conference on Power Electronic, Drives and Energy Systems, New Delhi, 2006, pp. 1-6.

25. R. K. Gupta, A. Somani, K. K. Mohapatra and N. Mohan, "Space vector PWM for a direct matrix converter based open-end winding ac drives with enhanced capabilities," 2010 Twenty-Fifth Annual IEEE Applied Power Electronics Conference and Exposition (APEC), Palm Springs, CA, 2010, pp. 901-908.

26. R. K. Gupta, K. K. Mohapatra and N. Mohan, "Open-end winding AC drives with enhanced reactive power support to the grid while eliminating switching common-mode voltage," 2009 35th Annual Conference of IEEE Industrial Electronics, Porto, 2009, pp. 700-707.

27. IEEE Guide for Identifying and Improving Voltage Quality in Power Systems," in IEEE Std 1250-2011 (Revision of IEEE Std 1250-1995) , vol., no., pp.1-70, March 31 2011

28. D. L. Sikes, "Comparison between power quality monitoring results and predicted stochastic assessment voltage sags-“real” reliability for the customer," in IEEE Transactions on Industry Applications, vol. 36, no. 2, pp. 677-682, Mar/Apr 2000.

29. M. H. J. Bollen, "Characterisation of voltage sags experienced by three-phase adjustable-speed drives," in IEEE Transactions on Power Delivery, vol. 12, no. 4, pp. 1666-1671, Oct 1997.

30. P. Heine and M. Lehtonen, "Voltage sag distributions caused by power system faults," in IEEE Transactions on Power Systems, vol. 18, no. 4, pp. 1367-1373, Nov. 2003.

31. L. Conrad, K. Little and C. Grigg, "Predicting and preventing problems associated with remote fault-clearing voltage dips," in IEEE Transactions on Industry Applications, vol. 27, no. 1, pp. 167-172, Jan/Feb 1991.

32. A. Van Zyl, R. Spee, A. Faveluke and S. Bhowmik, "Voltage sag ride-through for adjustable-speed drives with active rectifiers," in IEEE Transactions on Industry Applications, vol. 34, no. 6, pp. 1270-1277, Nov/Dec 1998.

33. J. L. Duran-Gomez, P. N. Enjeti and A. von Jouanne, "An approach to achieve ride-through of an adjustable-speed drive with flyback converter modules powered by super capacitors," in IEEE Transactions on Industry Applications, vol. 38, no. 2, pp. 514-522, Mar/Apr 2002.

34. Yong-Seok Kim and Seung-Ki Sul, "A novel ride-through system for adjustable-speed drives using common-mode voltage," in IEEE Transactions on Industry Applications, vol. 37, no. 5, pp. 1373-1382, Sep/Oct 2001.

35. A. von Jouanne, P. N. Enjeti and B. Banerjee, "Assessment of ride-through alternatives for adjustable-speed drives," in IEEE Transactions on Industry Applications, vol. 35, no. 4, pp. 908-916, Jul/Aug 1999.

36. Han Ju Cha and P. N. Enjeti, "A new ride-through approach for matrix converter fed adjustable speed drives," Conference Record of the 2002 IEEE Industry Applications Conference. 37th IAS Annual Meeting (Cat. No.02CH37344), Pittsburgh, PA, USA, 2002, pp. 2555-2560 vol.4.

37. C. Klumpner and F. Blaabjerg, "Experimental evaluation of ride-through capabilities for a matrix converter under short power interruptions," in IEEE Transactions on Industrial Electronics, vol. 49, no. 2, pp. 315-324, Apr 2002.

38. E. P. Wiechmann, R. P. Burgos and J. Rodriguez, "Continuously motor-synchronized ride-through capability for matrix-converter adjustable-speed drives," in IEEE Transactions on Industrial Electronics, vol. 49, no. 2, pp. 390-400, Apr 2002.

39. S. Tewari, R. K. Gupta and N. Mohan, "Three-level indirect matrix converter based open-end winding AC machine drive," IECON 2011 - 37th Annual Conference of the IEEE Industrial Electronics Society, Melbourne, VIC, 2011, pp. 1636-1641.

40. D. Orser and N. Mohan, "A Matrix Converter Ride-Through Configuration Using Input Filter Capacitors as an Energy Exchange Mechanism," in IEEE Transactions on Power Electronics, vol. 30, no. 8, pp. 4377-4385, Aug. 2015.

41. Mohan N. “Advanced electric drives: analysis, control, and modeling using MATLAB/Simulink”. John wiley & sons; 2014 Jul 22.

42. R. K. Gupta, K. K. Mohapatra, A. Somani and N. Mohan, "Direct-Matrix-Converter-Based Drive for a Three-Phase Open-End-Winding AC Machine With Advanced Features," in IEEE Transactions on Industrial Electronics, vol. 57, no. 12, pp. 4032-4042, Dec. 2010.

43. S. Tewari, R. K. Gupta, A. Somani and N. Mohan, "Indirect matrix converter based open-end winding AC drives with zero common-mode voltage," 2016 IEEE Applied Power Electronics Conference and Exposition (APEC), Long Beach, CA, 2016, pp. 1520-1527.

44. Iov F, Hansen AD, Sørensen PE, Cutululis NA. Mapping of grid faults and grid codes. Risø National Laboratory; 2007.